TIME-DEPENDENT RELEASE OF IRON FROM SOOT PARTICLES BY ACID EXTRACTION AND THE REDUCTION OF Fe^{3+} BY ELEMENTAL CARBON

A Thesis

by

STEPHEN JAMES DRAKE

Submitted to the Office of Graduate Studies of
Texas A&M University
in partial fulfillment of the requirements for the degree of

MASTER OF SCIENCE

May 2008

Major Subject: Mechanical Engineering

TIME-DEPENDENT RELEASE OF IRON FROM SOOT PARTICLES BY ACID EXTRACTION AND THE REDUCTION OF Fe^{3+} BY ELEMENTAL CARBON

A Thesis

by

STEPHEN JAMES DRAKE

Submitted to the Office of Graduate Studies of
Texas A&M University
in partial fulfillment of the requirements for the degree of

MASTER OF SCIENCE

Approved by:

Chair of Committee, Bing Guo
Committee Members, Don Collins
William Marlow
Head of Department, Dennis O'Neal

May 2008

Major Subject: Mechanical Engineering

ABSTRACT

Time-Dependent Release of Iron from Soot Particles by Acid Extraction and the Reduction of Fe^{3+} by Elemental Carbon. (May 2008)

Stephen James Drake, B.S., Texas Christian University

Chair of Advisory Committee: Dr. Bing Guo

Elemental carbon reduces Fe^{3+} to Fe^{2+} in aqueous solutions. This process has potential implications in the adverse health effects of fine particles in air pollution, because both elemental carbon and iron are major components in atmospheric particulate matter. In this study we measured the time-dependent release of iron from laboratory flames and standard reference soot particles that contained iron, and the reduction of Fe^{3+} to Fe^{2+} in an acid extraction process. The concentration of Fe^{3+} and Fe^{2+} ions in the extraction solutions was measured by a spectrophotometric method. The results showed that while Fe^{3+} was the dominant valence state in the dry soot particles, significant fraction of iron was reduced to Fe^{2+} in the aqueous solution. Further investigation is needed to assess the significance of this phenomenon in the biological effects of particles that contain iron and elemental carbon.

DEDICATION

This work is dedicated to my love, Megan. Her love and support are my inspiration for all that I do. Her patience and understanding have allowed me to put the time and effort needed into this project. To my parents, Steve and Karen, for their encouragement and love that set the foundation from which I build my life. To my sister, Heather, who has supported me throughout my academic journey and for our shared respect for each other. To my grandparents, Herb and Jean, for their presence in my life. They inspire me each and every day for all they have accomplished, what they stand for, and their desire to be involved in all that I do. And to Paul and Sheila, who always offered a home and family away from my own.

ACKNOWLEDGEMENTS

I would like to thank Dr. Bing Guo, who gave me an opportunity to work on this project; this was an incredible learning opportunity and I utterly appreciate his guidance throughout this experience. I would also like to thank the members of my committee, Dr. Don Collins and Dr. William Marlow, for their time and insight. To those people in and around the laboratory, especially Brandon Tompkins, Mallika Mukundan, and Hoon Yim, their daily help made things possible. Special thanks to Dr. Abraham Clearfield and Dr. Boris Shpeizer in the Texas A&M Chemistry Department for their concurrent work performing BET surface area analysis, Don Poe of the NRG Limestone Power Generation Plant for providing coal fly ash samples, Grace Prindle of Degussa Corporation (recently renamed Evonik Industries) for providing Printex 90 samples, and Airat Khasanov from the University of North Carolina at Asheville for Mössbauer spectroscopy analysis.

Funding for this study was provided by Texas A&M University and Texas Engineering Experiment Station.

TABLE OF CONTENTS

Page

Page

LIST OF FIGURES

Page

Page

Page

NOMENCLATURE

B-CFA	Baked Coal Fly Ash
C_2H_2	Acetylene
C_2H_4	Ethylene
CFA	Coal Fly Ash
Degussa+Fe_2O_3	Degussa Carbon Black with Iron Oxide Mixed In
DI water	De-ionized water
Fe^{2+}	Iron with an oxidation number of two, i.e., two electrons lost and positively charged
Fe^{3+}	Iron with an oxidation number of three, i.e., three electrons lost and positively charged
$Fe(CO)_5$	Iron Pentacarbonyl
Fe_2O_3	Laboratory Generated Iron Oxide
$FeSO_4$	Iron (II) Sulfate Hydrate
NIST Diesel	National Institute of Standards and Technology Standard Reference Material 2975, Diesel Particulate Matter
SCFH	Standard Cubic Feet per Hour
Soot-A	Laboratory Generated Acetylene Soot
Soot-A+Fe_2O_3	Laboratory Generated Acetylene Soot with Iron Oxide Mixed In

Soot-E	Laboratory Generated Ethylene Soot

INTRODUCTION

Iron is the fourth most abundant element in the earth's crust. It has been measured in every aspect of our atmosphere from fog, snow, cloud water, and rain at several different locations (Zhuang et al. 1995). Iron and elemental carbon are two ubiquitous major components of airborne particulate matter (Cass et al., 2000). Iron is thought to exert toxicity due to its ability to produce reactive oxygen species through the Fenton reaction (Smith et al., 2000; Van Maanen et al., 1999). Iron exists in two different oxidized forms, namely ferrous iron, Fe^{2+}, and ferric iron, Fe^{3+}. The ability of iron to generate hydroxyl radicals, OH, is highly dependent upon the oxidation state of the iron. Fe^{3+} does not generate detectable OH radicals unless a reductant is present to reduce the iron to Fe^{2+}. Therefore it is important to determine the oxidation state of iron from particles when studying their health effects. This dependence is due to the Fenton oxidation reaction. It is considered to be one of the most powerful oxidation reactions and can be used to degrade various organic compounds because of existence of OH which is known as one of the most active oxidants and has a higher oxidation potential than other oxidants. It is thought that OH is generated by reaction of hydrogen peroxide, H_2O_2, and Fe^{2+}, which acts as a catalyst.

This thesis follows the style of *Aerosol Science and Technology.*

1) $Fe^{2+} + H_2O_2 \rightarrow Fe^{3+} + OH^{\bullet} + OH^-$

2) $Fe^{3+} + H_2O_2 \rightarrow Fe^{2+} + OOH\bullet + H^+$

3) $Fe^{2+} + HO^+ \rightarrow Fe^+ + OH^-$

4) $HOO^{\bullet} + Fe^{3+} \rightarrow Fe^{2+} + O_2 + H^+$

5) $HO^{\bullet} + H_2O_2 \rightarrow HOO^{\bullet} + H_2O$

6) $Fe^{2+} + HOO^{\bullet} \rightarrow Fe^{3+} + O_2H^-$

This reaction allows iron to interact independently with others metals. Alone or combinations of Fe^{2+} can damage cell membranes and rearrange DNA structures, which disrupts cellular functions (Bruins et al., 2000; Brewer, 2006; Filho et al., 1983; Tuomainen et al. 2007); this is explained in greater detail by Weinberg (2007).

Oxidation of activated carbon fibers release carbon dioxide, CO_2, and H^+, with no carbon monoxide detected. The measured amount of CO_2 should agree with the amount of Fe^{3+} being reduced. While the release of the gas is of proper note, it is still a small part of the redox reaction. Although Fu et al. (1993) used different metals the general mechanism should be similar. We would also expect carbon dioxide gas release during the acid extraction process.

Iron and elemental carbon are two major constituents in coal fly ash (Veranth et al., 2000). Even with the emission control technology, some coal fly ash still passes through the stack and enters the atmosphere. The coal fly ash captured by the emission control equipment may still pose a workplace hazard during handling. Ultrafine particulate matter, similar to coal fly ash, appears to have high redox activity (Cho et al., 2005; De Vizcaya-Ruiz 2006) in addition to reported positive

correlation between the redox activity of airborne particulate matter and its elemental carbon concentration (Cho et al., 2005; Geller et al., 2006). Epidemiological data have shown that inhalation of fine and ultrafine particles cause various adverse health effects (Samet et al., 2000; Dockery et al., 1993; Oberdorster, 2001; Oberdorster et al., 1995; Schwartz and Neas 2000).

Emission from motor vehicles contains a high fraction of elemental carbon (Table 1), as well as significant amount of metals, including iron (Huggins et al., 2000).

Table 1. Adapted from Geller et al., 2006, that shows trace element emissions from different sources.

Emission rates of PM mass (mg km^{-1}), elemental and organic carbon and selected PAH species (ng km^{-1})

Component	Diesel transient	Diesel SS[a]	Gasoline	Gasoline SS[a]	Cat DPF transient	Cat DPF SS[a]
Mass (mg km^{-1})	25±6	14	5.8±0.3	0.4	1.0±0.1	0.4±0.1
Elemental carbon (EC)	12911±335	7095	473±134	13	137±66	67±40
Organic carbon (OC)	4967±1687	5751	1462±491	375	482±45	230±78
Naphthalene	217±73	201	15±5	1.9	1.7±1.4	ND[b]
Phenanthrene	285±88	61	39±16	3.4	7.3±1.7	4.0±0.2
Anthracene	7.6±2.4	5.1	5.4 ±1.9	0.4	0.3±0.3	ND[b]
Fluoranthene	12±5.4	ND[b]	43±12	5.3	12±1.7	5.8±3.2
Pyrene	161±21	107	48±12	5.4	26±3.2	9.6±6.6
Benz(a)anthracene	5.0±0.8	1.2	23±4.2	17.0	13±5.0	6.4±1.0
Chrysene	6.1±0.4	1.7	31±4.4	27.7	17±4.3	11±1.2
Benzo(b)fluoranthene	0.7±0.2	ND	6.7±0.5	1.2	7.0±5.4	1.8±0.8
Benzo(k)fluoranthene	ND[b]	ND	1.6±0.4	0.5	ND	ND
Benzo(a)pyrene	ND	ND	4.2±0.4	0.3	0.2±0.2	ND
Benzo(g)perylene	ND	ND	7.7±2.9	0.3	ND	ND

Standard deviations are presented when multiple tests have been averaged.
[a]SS = steady state.
[b]ND: below the limit of detection.

Combustion derived nanoparticle are the dominant particle type in the urban atmosphere, which provide a key component since they contain a large surface area, organics, and transition metals. The common relationship between these parameters is their ability to generate oxidative stress in lung cells that can cause lung injury (Donaldson et al., 2005).

Since their inception in 1991, there has been an increase in interest with carbon nanotubes due to their structural, electronic, and mechanical properties (Iijima, 1991). These carbon nanotubes carry metal catalysts including iron (Lam et al., 2006). As the use of nanomaterials becomes increasingly popular, significant exposure to it may be expected for the public or in the workplace (Oberdorster et al., 2005). Concerns about the human health impacts of engineered nanoparticle materials have initiated studies relevant to biological systems. Such studies are aimed toward mimicking industrial environments to hopefully gain understanding on the long term toxicity of such interaction (Limbach et al., 2007).

Iron in airborne particles exists in both water-soluble and insoluble forms. Both forms of iron and in the particulate matter can become bioavailable (Majestic et al., 2006). In fact, much of the iron in ambient particulate matter is insoluble in water (Fernandez et al., 2003). Literature indicates that insoluble iron in particles can become bioavailable and cause the adverse health effects (Knaapen et al., 2002). Therefore, when measuring the amounts and oxidation state of bioavailable iron, both the water soluble and insoluble forms should be included.

Despite this importance of the oxidation state of iron, few measurements of the oxidation state have been done (Fenoglio et al., 2001; Prandi et al., 2001; Veranth et al., 2001; Zhou et al., 2003, Majestic et al., 2006). Therefore the concentration, speciation, and reactivity of Fe^{2+} and Fe^{3+} will, in turn, pose significant implications on the speciation, toxicity, and mobility of other contaminants and trace metal.

The following research has strong potential to bring significant benefits to

the air quality research community through its impact in future collaborative research. It addresses an important aspect of air pollution with a simple and unique approach. This may prove to become a simple, economical, and reliable procedure for assessing the health impact of airborne particles on the basis of iron toxicity. Most importantly, it will provide useful information that is currently lacking within the current air quality community.

OVERVIEW OF MATERIALS

NIST Diesel sample was purchased from the National Institute of Standards and Technology, labeled Standard Reference Material 2975, Diesel Particulate Matter. This was used so that anyone trying to replicate this study would have a common repeatable place to start.

The Degussa sample, more specifically Printex 90, was donated for educational/research purposes by the Degussa Corporation. As of 12 September 2007 this company will now be known as Evonik Industries. Evonik's is based in Essen, Germany. Its largest plant in the United States is in Mobile, Alabama.

The coal fly ash samples were donated by the NRG Limestone Power Generation Plant in Limestone County near Jewett, Texas.

Acetylene soot, Soot-A, ethylene soot, Soot-E, and iron oxide, Fe_2O_3, were generated in a laboratory environment at Texas A&M University. Fe_2O_3 was created to be mixed with Soot-A and the Degussa carbon black after it was generated.

The baked coal fly ash, B-CFA, was created by taking CFA from the donated sample, and placing it into the Barnstead Thermolyne Tube Furnace (Model 21100, See Appendix C).

EXPERIMENTAL PROCEDURE

For all procedures the following conditions remained constant. Chemicals were reagent grade or better. All glassware and plastic bottles were acid washed with DI water rinsed several and air-dried prior to use. De-ionized water, DI water, was obtained from the physics department via a Millipore Milli-Q and Milli-RO Ultrapure Water Purification System. All reagent preparation and experiments were conducted in an ambient atmosphere at room temperature which was kept near constant at 25 °C.

Initial Equipment Testing

The integrity of the test tubes and cuvettes were analyzed to ensure repeatable measurement readings. The Cole-Parmer Spectrophotometer (Model 1100, Serial Number: CS0509095) wavelength was set to 512 nm and turned on and allowed to become steady state for no less than 60 minutes, based off manufacturers standard operations recommendations.

Twelve test tubes and nine cuvettes were filled with DI water and were then measure for their respected absorption. Each time data was collected the spectrophotometer was zeroed with the same test tube or cuvette. The order of measurement was kept the same for all tests. The test tube tests were done first, measuring all twelve test tubes and the repeating two times. Then all nine cuvettes

were measured and the also repeated two times. A few times, and only for the test tubes, the initial number was displayed and then it started to decreased until a final number was determined. The repeatability graph is shown in Figure 1.

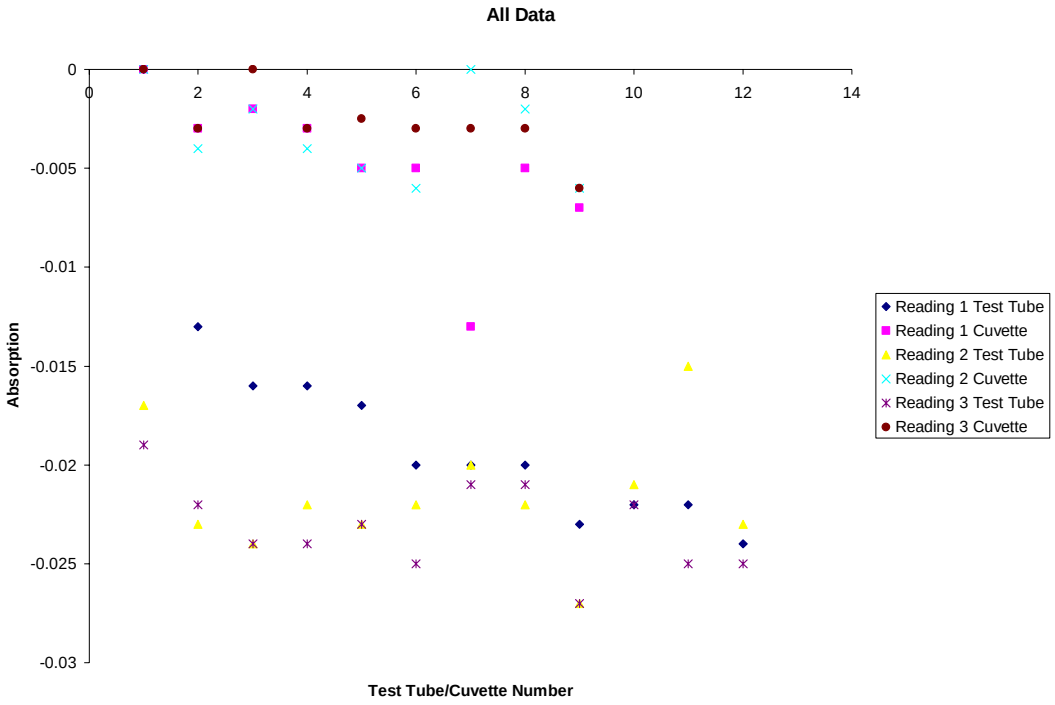

Figure 1. All data for test tube and cuvette comparison.

Based on these results it was decided that only a single cuvette would be used to analyze a solution. With more confidence in the data the calibrations curve was now ready to be constructed.

Calibration Curve

For the stock $FeSO_4$ solution approximately 0.05 g of pure iron (II) sulfate hydrate was weighed using Scientech Scale (Model ZSA-80, Serial Number: 25229, See Appendix B) to the nearest 0.1 mg and transferring to a 1 L volumetric flask. 200 mL of DI water was added and shaken to dissolve any remaining solids. 20mL of 20% sulfuric acid was added to the solution, it was then dilute to the 1 L mark. A series of standards were created by pipetting into each of five 100 mL volumetric flasks; 1.00, 5.00, 10.00, 25.00, and 50.00 mL aliquots of the stock Fe^{2+} solution. Into a sixth, 100 mL volumetric flask, 50 mL of DI water was used to serve as a blank. Into a seventh, 100 mL volumetric flask, 10mL of stock Fe^{2+} solution was added. In sequence to all of the solutions, 1 mL of 1% in hydroquinone was added except the seventh flask, then 10 mL of 0.3% 1, 10-phenanthroline solution in water with 10% acetone. The solutions were diluted to the 100 mL mark in volumetric flasks, mixed thoroughly, and allowed to stand for 60 minutes for color development show in Figure 2**.**

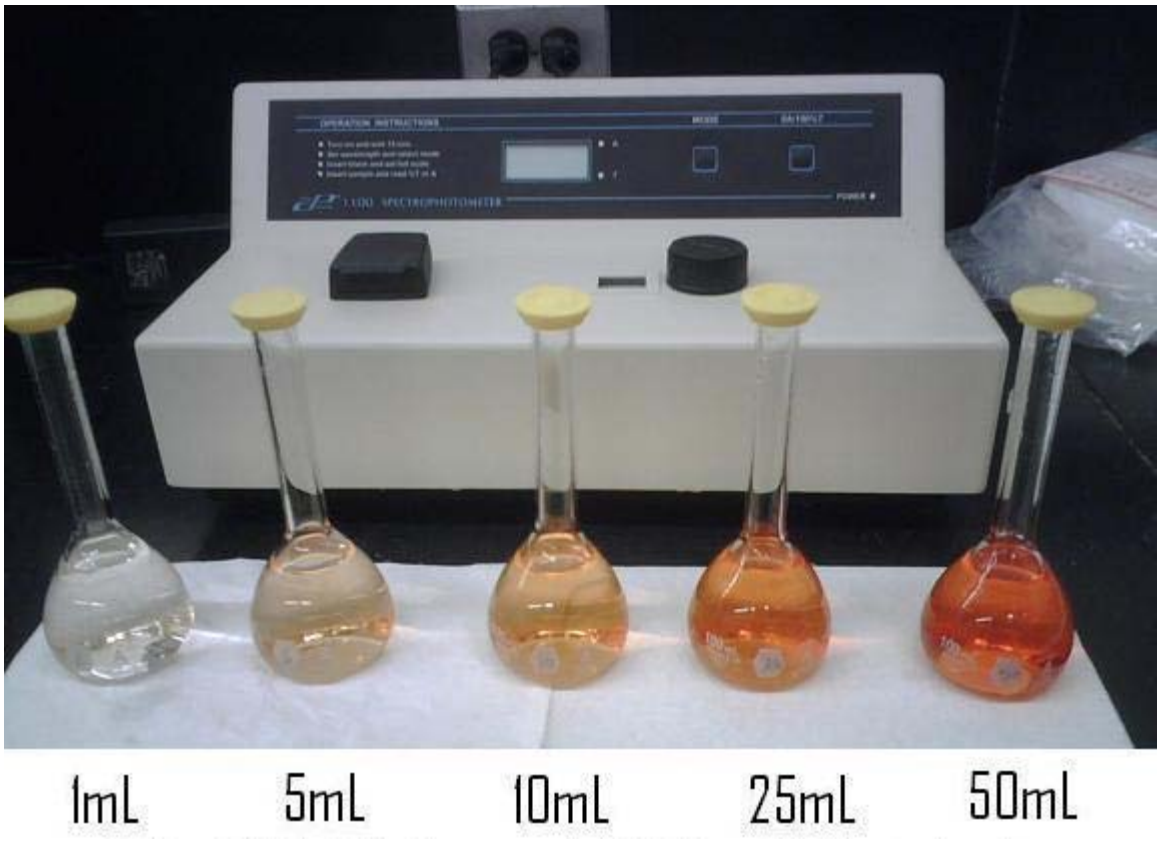

Figure 2. Complete color development for different $FeSO_4$ solution volumes.

Allowing spectrophotometer to warm up for at least 60 minutes DI water, was placed into a scratch-less, clean cuvette. The reset button, 'OA/100%T', was depressed allowing the machine calibrate itself with a base solution of zero absorbance. Then solution to be tested was placed into a cuvette, and the absorbance was recorded. After each measurement the cuvette was washed with DI water and the machine was recalibrate using the aforementioned method. This was done for the next three 15 minute intervals. Figure 3 appears to show only a single data point at the different volume amounts, however upon closer inspection, three measurements are revealed, proving that the color development has stabilized.

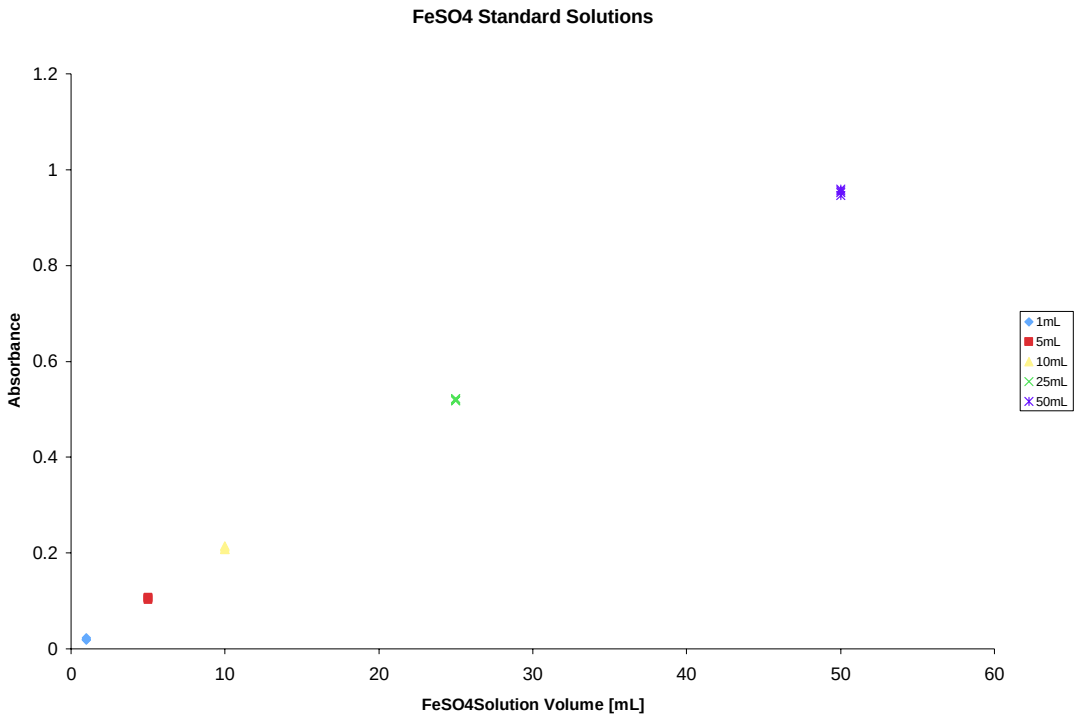

Figure 3. Calibration curve.

The seventh flask was essentially the same as the corresponding standard, suggesting that not adding hydroquinone did not change the outcome dramatically. The calibration curve for the spectrophotometer was to both ensure its correct operations and also a means for determining unknown concentrations later.

For soot generation an MKS Multi Gas Controller (Model 647C-4-R-O-N, Serial Number: G105266G40) would be used for our fuel/carrier gas and co-flow gas. Within this machine a correction factor number is associated with each gas. During initial tests Acetylene, C_2H_2, was used and a corresponding number was available; however further into testing Ethylene, C_2H_4, began being used. Neither the company's website nor company literature gives this value for C_2H_4, Ethylene. The

mass flow controller's manuals given an equation to help determine this number, but not all the values were listed to help finalize a number. Ultimately, technical services were reached and a number was agreed upon; 0.60 for C_2H_4.

Soot Generation

Laboratory samples were created using a flame system that generated soot particles. C_2H_4 or C_2H_2 were transported from the cylinders using either a Harris Two Stage Regulator (Model 9296NC) for C_2H_2 or a Harris Single Stage Regulator (Model CGA E4 425-125A) for all other gases. The fuel gas was split into two gas lines and was routed via the mass flow controllers and through MKS Mass Flo Controller Modules (Model 1179A14C51BV). One line was directed to Iron Pentacarbonyl, $FeCO_5$, which contains the desired metal, and was subjected to a chilled water bath to alter the saturation vapor pressure following the Clausius-Clapeyron relation Fuel gas flows through this chemical and was paired with the pure fuel gas line toward the burner and formed a laminar diffusion flame at the burner mouth which was supported by the co-flowing stream. The integrity of the co-flow stream was tested and was determined not to change the sample's properties. Evidence of the co-flow stream addition to the stability to the flame is evident when comparing the images in Figure 4**.**

Figure 4. Initial soot generation setup with co-flow head (left); flame without co-flow head.

The post flame aerosol was then directed toward a sampling tube attached to Edwards RV Rotary Vane Vacuum Pump. Inside the sampling tube either a Whatman Anodisc 47 mm, .2 µm filter or an Advantec MFS Borosilicate Microfiber 47 mm, .2 µm glass filter used to capture the soot. The schematic of the flame synthesis apparatus is shown in Figure 5. Depending on the operating parameters, Fe_2O_3 nanoparticles, soot particles, or soot particles with metal impurities can be generated with this apparatus.

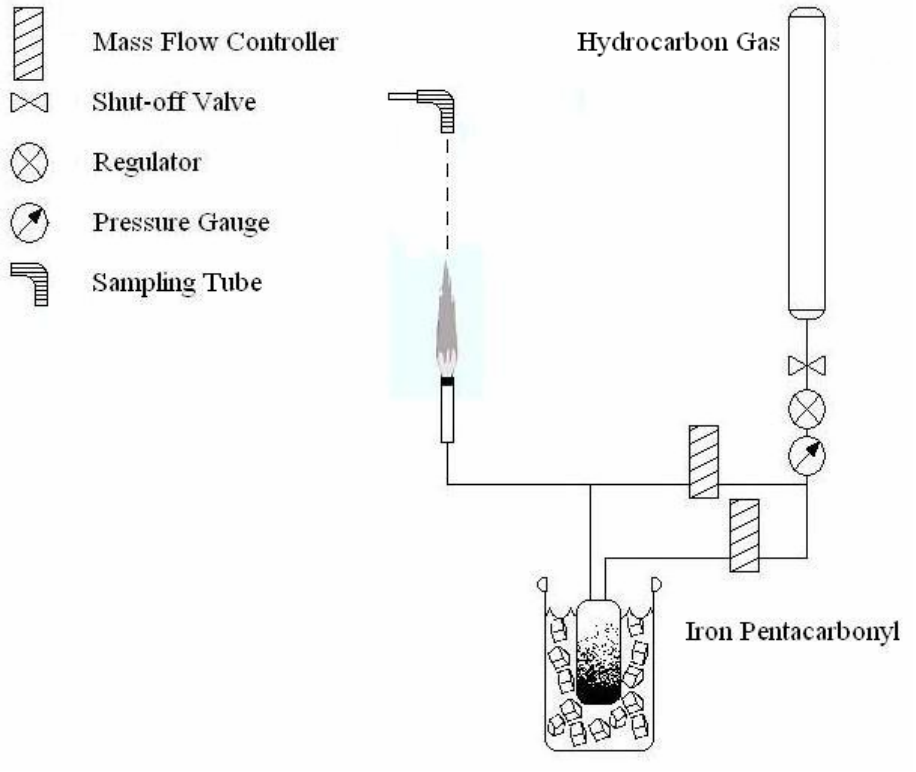

Figure 5. Laboratory soot production setup.

While this setup was used in nearly 95% of the soot generation cases, it needed to be upgraded. In a typical testing environment, a soot sample test would take 2 hours and produce 75 mg to 120 mgs. This system was inefficient and upon observation, most of the soot looked to be going out the exhaust duct. The main factor attributed to this was the laboratory environment was not air tight. This played havoc with keeping the flame stable and then capturing the soot. Since the environment could not be changed, the sampling equipment was adjusted. The small 1/4 in. diameter nozzle and 47 mm filter holder was replaced with a custom made ½ in. diameter nozzle and 4 in. Hi-q Filter Holder (Model: ILPH-102) using Hi-q Weighted Filters (Environmental, Part Number: FP5211-102), see Figure 6.

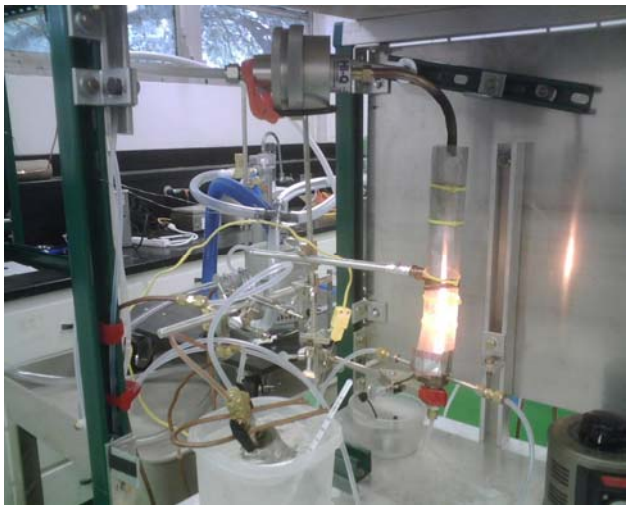

Figure 6. New soot collection system.

Additionally, the vacuum pump was replaced with an Ametek Thermally Protected Motor (Model: 117416-00 RCFT). This stronger motor was required because of the surface area increase in order to ensure isokinetic sampling. A Dwyer Air Meter (Model: Rmc-101 T27P) was added to determine the post collection flow rate and a Deltrol Easy Read Flow Regulator (Model: EN 30 B) allowed control of this flow rate, all shown in Figure 7.

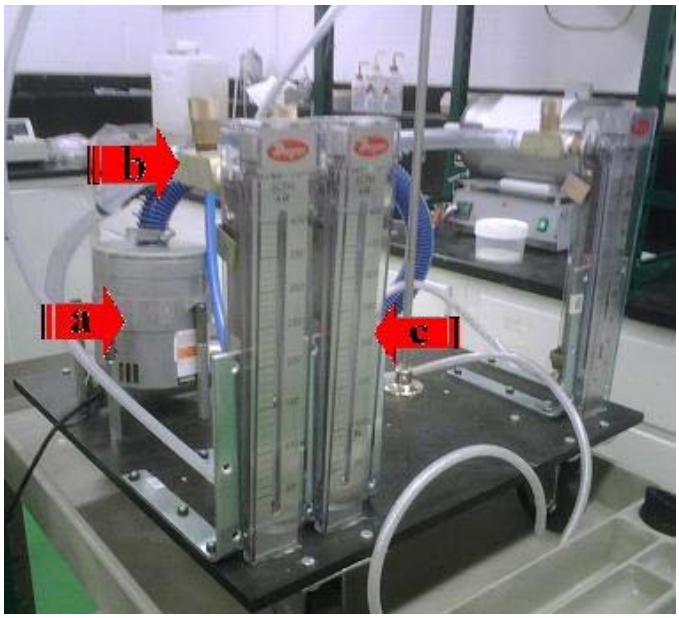

Figure 7. New soot collection equipment, Ametek motor (a); Deltrol regulator (b); Dwyer air meter (c).

A mesh tube was occasionally placed around the flame to add stability. Its presence was noticeable when several persons were performing experiment or when the laboratory door had to be kept open. The new soot generation system improved collection efficiency by over 300%. Depending on the type of soot being produce, 90 mg to 1000 mg samples were created in no longer than 30 minutes. The sample time duration dramatically decreased because the soot buildup over the larger surface area placed a large strain even on the newer more powerful motor. An importance was placed on watching the air meter. The beginning of the experiment, and average flow rate was about 190 SCFH and after only 30 minutes it dropped to 50 SCFH. Requiring the motor to run at a low flow rate (low pressure) over an extended time might be detrimental to such equipment.

The filter housing was then disassembled and the soot contents were weight and properly labeled for later use.

Acid Extraction

The scale was turned on and allowed for warm up for no less than 60 minutes. The samples were weighted, placed in a beaker, and properly labeled. To that beaker, 20 mL 20% sulfuric acid was added and if the sample did not wet completely, 5 mL isopropyl alcohol was added. DI water was added to the solution to make the total volume 100mL.

That solution was then heated via a Revolutionary Sciences Poly ProBath (Model RS-PB-100, See Appendix B) filled with DI water. This was done for different time durations and temperature of 40 °C and 80 °C respectively. 40 °C was chosen for its proximity to that of the human body of 37 °C, so that inference could be made on a physiological basis. 80 °C was chosen to simulate and extend test at 40 °C. After the allowed time, the solution was transferred to a 1 L volumetric flask through a filter. The solution was then diluted to the 1 L mark with DI water.

The filtered soot was placed in a Petri dish so future analysis could be done on the post acid extraction sample.

Acid Extraction Analysis

The spectrophotometer was set to a wavelength of 512 nm and turned on then allowed for warm up for no less than 60 minutes. 50.00 mL of the 1 L solution was pipetted into two 100mL volumetric flask labeled “A” and “B”. To flask “A” 1 mL

of 1%, hydroquinone water solution was added shaken well and allowed to sit for 1 minute. Then to both flasks 10 mL of 0.3% 1, 10-phenanthroline 10% acetone solution was added. The 1, 10-phenanthroline was allowed to completely dissolve in the acetone solution first, then the remaining calculated DI water volume was added to obtain the final specified concentration. Both solution were diluted to the 100 mL mark, mixed and shaken thoroughly, and then left to stand for 60 minutes. DI water is pipetted into a cuvette to reset the spectrophotometer. Once the spectrophotometer read a constant zero, the water was be dumped out and the solution analysis could be performed. The same cuvette was used and washed for every measurement. A sample from flask "A" is pipetted into the cuvette and the absorbance is read and recorded. The cuvette is emptied in an environmental hazard and safety approved chemical disposal container, and the procedure is then repeated for flask "B." After each round of measurements the spectrophotometer is reset with DI water before another round of data is recorded. Data was recorded in quadruplicate to ensure that the measurements are accurate; this procedure results in Flask "A" yielding the absorbance for total Fe and flask "B" the absorbance for Fe^{2+}. These numbers were then compared to the spectrophotometers calibrations curve to determine the concentration of the solutions as well as other measurements. Standard curves were developed for each sample after each acid extraction.

BET Surface Area Measurement

Prior to the surface area analysis, all samples to be tested were placed in the tube furnance at 250 °C for 24 hours in order to reduced the moisture content of the sample allowing for a faster and more accurate measurement.

The BET surface area measurement was applied on three different soot samples: Degussa+Fe_2O_3, Soot-E, and NIST Diesel. A glass tube, or cell, that the sample will be analyzed in, was weighted first as in Figure 8 (left).

Figure 8. Soot sample preparation (left); front of degasser (middle); cell inserted with heated bag below (right).

Then the sample was placed within the cell, weighted again to determine the sample mass, then the assay was ready to commence. Since there was not a definitive estimate on what the final surface area would be for the samples, the smaller of the two types of cells were used. It was chosen based on the hypothesis that the sample might be relatively low in density, and the smaller cell would allow for a shorter test period. It was later concluded that the larger cell was needed to acquire the proper reading.

Once the proper cell size is determined and the sample is correctly weighed, the cell is inserted into Quantachrome Autosorb Degasser. This instrument fills the cell with helium, and then begins to evacuate the cell of all gas. During this process, a heated ceramic bag is placed around the cell to speed up the vacuum process and eliminate any remaining moisture shown in Figure 8 (right).

Upon the completion of this process, the cell is then is placed into the Quantachrome Autosorb-6 Analyzer where it will be filled with nitrogen, while the outside of the cell it placed into a liquid nitrogen bath, see Figure 9. Then gas sorption-desorption isotherms will be obtained under following programmed instrument cycles. Lastly, the instrument will calculate the surface area of the sample.

Figure 9. Quantachrome Autosorb-6 Analyzer

Mössbauer

Mössbauer spectroscopy is a spectroscopic technique based on the Mössbauer effect. A solid sample is exposed to a beam of gamma radiation, and a detector measures the intensity of the beam that is transmitted through the sample. This will change depending on how many gamma rays are absorbed by the sample. The Mössbauer effect is that a significant fraction of the gamma rays emitted by the atoms in the source do not lose any energy due to recoil and thus have almost the right energy to be absorbed by the target atoms. The output is spectra of data, where gamma-ray intensity is plotted as a function of the source velocity. Gamma-rays are absorbed, resulting in a drop in the measured intensity and a corresponding dip in the spectrum. The number, positions, and intensities of the dips provide information about the chemical environment of the absorbing nuclei and can be used to characterize the sample (Miglierini and Petridis, 1999).

Samples were sent to Airat Khasanov from the University of North Carolina at Asheville to conduct Mössbauer Spectroscopy analysis.

RESULTS AND DISCUSSION

BET analysis, see Figure 10, quickly shows the sample's surface areas relative to each others. Degussa was noticeably the largest with 354.5 [m^2/g], while Diesel and Soot-E were clustered closer at 118.7 and 181.8 respectively. The larger the surface area would suggest the sample would dissolve in the solution faster and allow for greater locations where Fe could interact with elemental carbon to reduce Fe^{2+}.

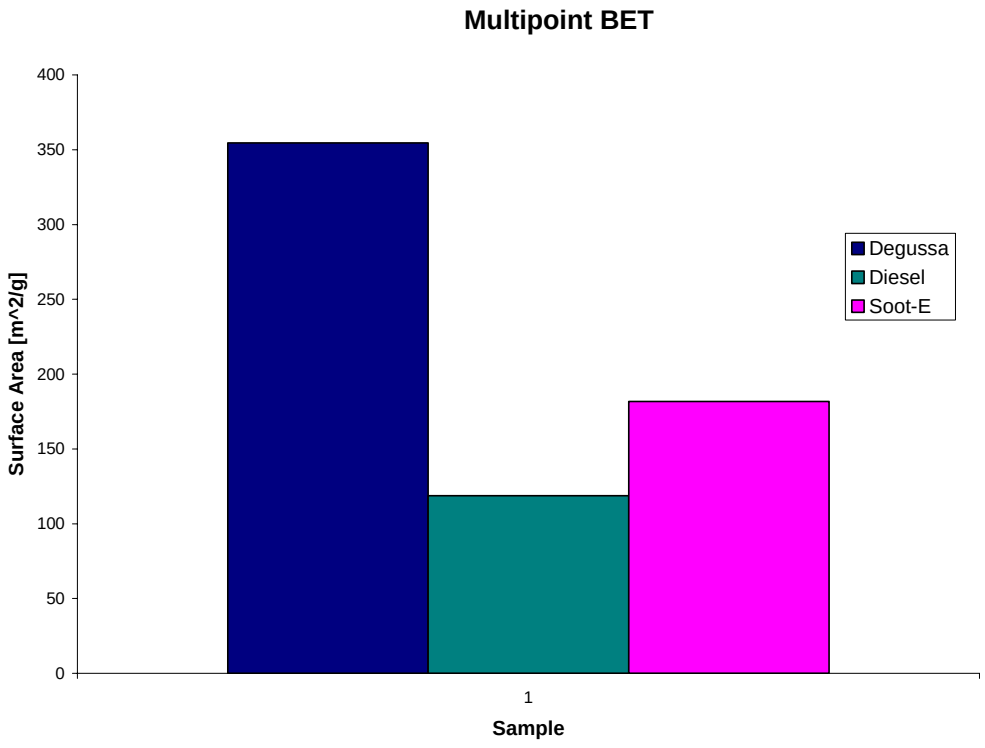

Figure 10. BET graphically representation of data.

It should first be noted that the Degussa+Fe_2O_3, Soot (Ethylene), CFA, and B-CFA data points represents the average of analysis repeated in triplicate, while time only allowed for Soot (acetylene), Soot (Acetylene)+Fe_2O_3, and NIST Diesel to be analyzed once.

Figure 11 below shows the Fe mass of iron dissolved with acid extraction done at 80C. The data appears to have a relative unchanging concentration of iron. The two main exceptions can quickly be assumed to show a false scenario of the samples true nature. The final point of B-CFA and the fourth point of Soot (Acetylene)+Fe_2O_3, seem to be unreasonably high, but this is thought to be due to the single analysis. The only exception of note would be the second data point in the ethylene soot sample. It suddenly spikes and then returns near the averages of its others. It also it thought to be uncharacteristic of the total sample. The data have a mass fraction range from near zero to about 2.5%. The most dramatic changes happen between the first two data points.

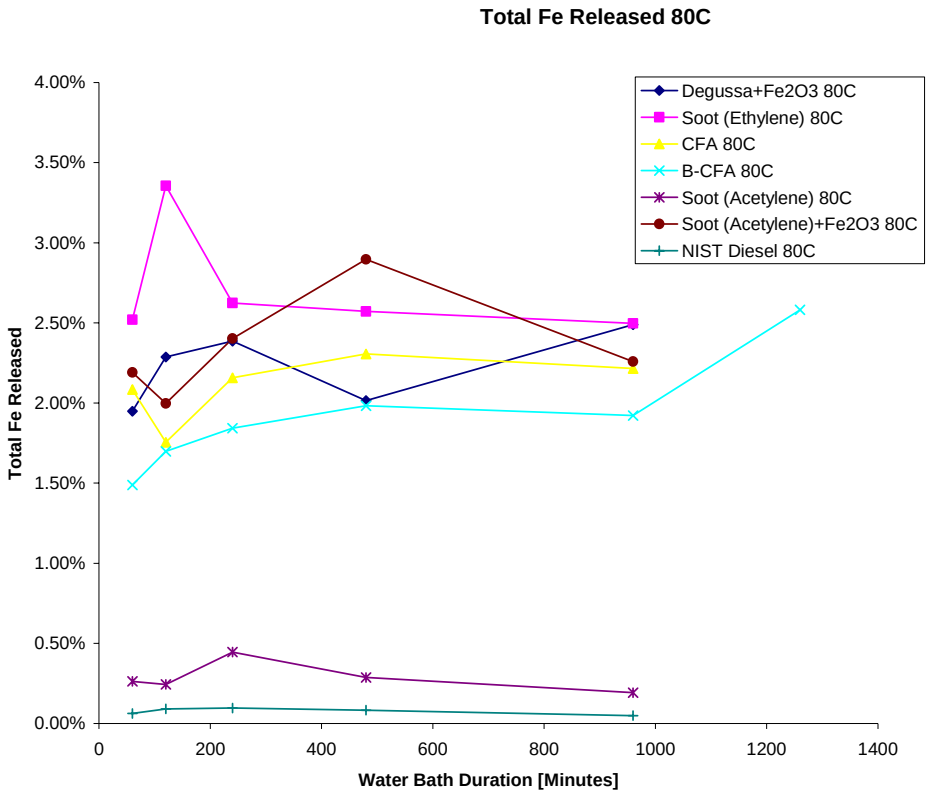

Figure 11. Total Fe released in different samples following acid extraction at 80 °C.

Next, Figure 12, is the Fe mass dissolved by acid extraction done at 40C. Its shape is somewhat different to its predecessor. Some samples show a flat line, while others grow in an exponential manner only to level off in the end. Both graphs taken separately might seem to be unrelated and would warrant no correlation. However, when placed next to each other, the 40C on the left and the 80C on the right (See Figure 13), with the same y-axis scale, a pattern starts to become apparent. The graphs show how fast Fe is dissolved from the samples into the solutions. This should be analogous to the speed at which Fe can become bioavailable in biological conditions.

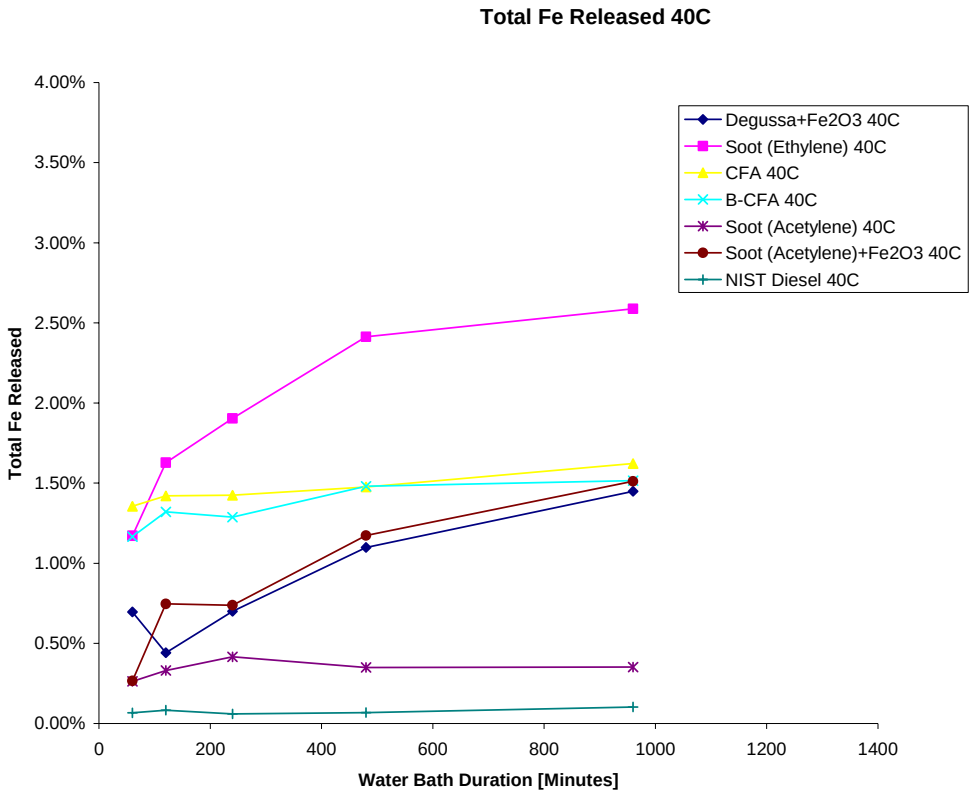

Figure 12. Total Fe released in different samples following acid extraction at 40 °C.

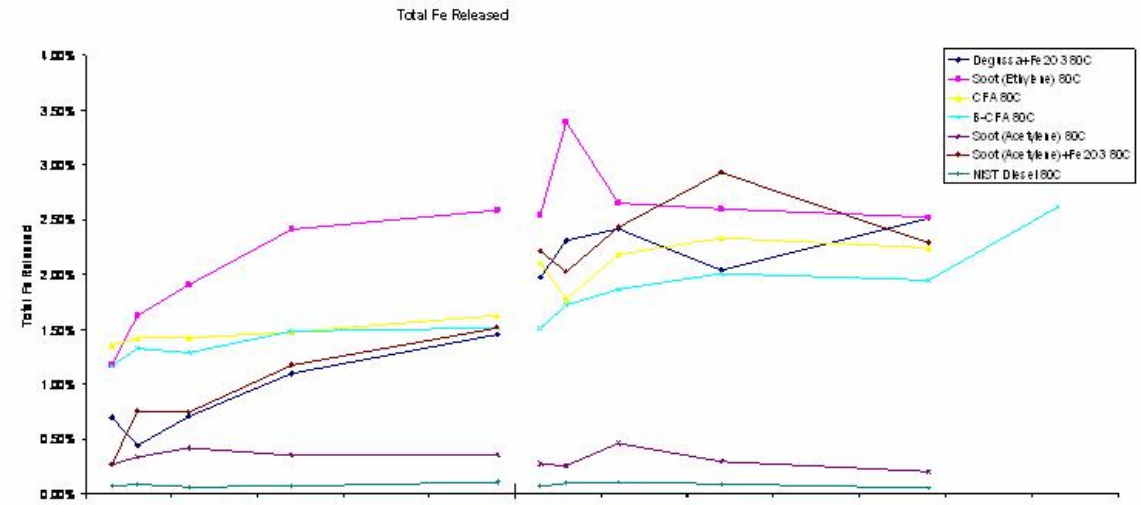

Figure 13. Extended view of the amounts of total Fe released.

It is this author's view that while the shapes may appear to be different, the final result will be the same. In the 40 °C case, the Fe dissolved, for most samples, takes a little over 8 Hours, 500 Minutes, to reach equilibrium. While the 80 °C equilibrium is either immediately obtained or is reached quickly. This is attributed to the acid extraction solution temperature. When the sample solution is placed into the hot water bath, the solution itself is at room temperature. For a 40 °C test, the temperature of the acid solution takes over an hour and a half to reach 40 °C, compared to 30 minutes in the 80 °C case. For NIST Diesel and Soot-A, temperature seems to have no effect. B-CFA and CFA did not respond at low temperature and only a little more at the higher temperature. If the 40 °C were allowed to run indefinitely, it is believed that the shape and final concentrations would mimic the graph above.

In the case of Fe^{2+} concentration a small difference is of more importance. Figure 14 shows that at 80C, in most samples, there is a noticeable increase in the amount of Fe^{2+} being produced initially, with a small decrease later. As expected, B-CFA and CFA do not change much due to the lack of inherent carbon to drive the reduction in spite of its sizeable Fe total. The only surprise was the initial decrease of Fe^{2+} in the CFA case. It could be surmised that either the first point was too high or that the second point was too low, but it would be expected to behave similar to the others.

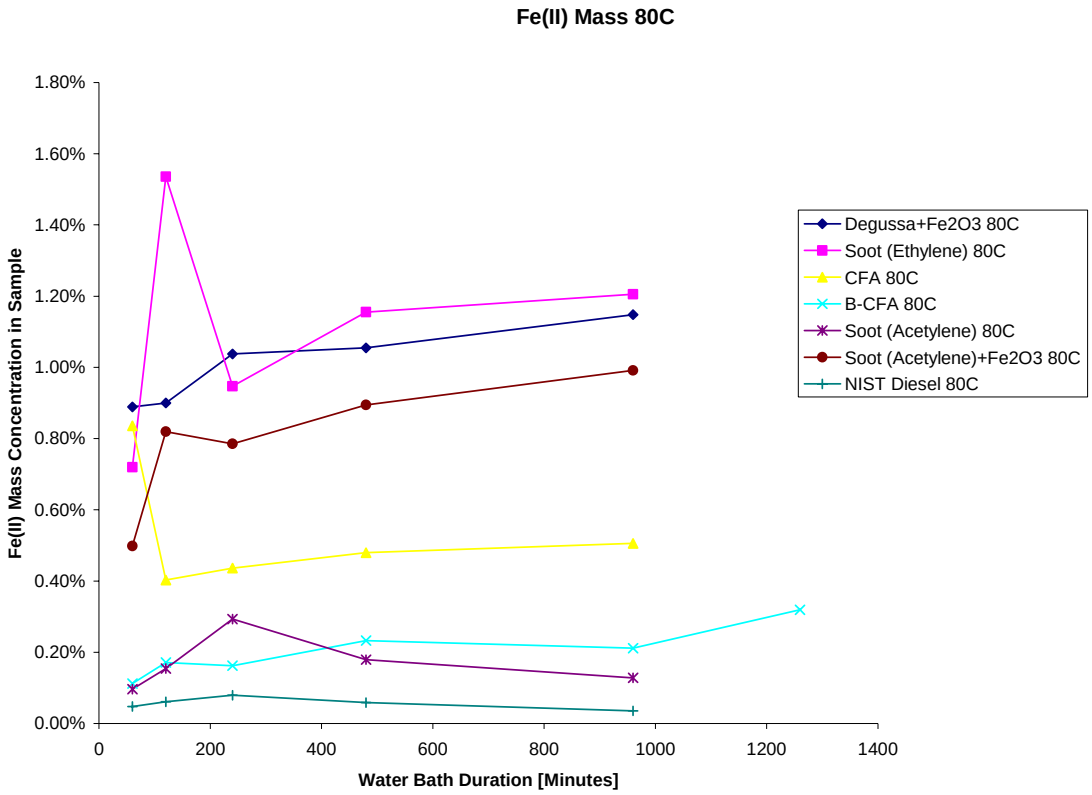

Figure 14. Fe^{2+} concentrations of different samples following acid extraction at 80 °C.

Fe^{2+} concentration at 40 °C didn't appear to look the same, see Figure 15, but they can be thought as similar. Most samples had an initial increases, but then seemed to taper off. This is not thought to be a fluke.

While the graph appears to decrease or level off it does not give the entire scope of what is happening. As the process goes on, more and more iron is being dissolved into the solution. Initially, the surface area of the sample is large enough to allow for this intense reduction of Fe. As this process continues, Fe is still being dissolved but the rate at which the Fe is being reduced decreases, making the ratio decrease and the graph appear to decline. No matter how this is interpreted, the main point that must not be overlooked is that the first hour is the most critical time for

this reduction to occur. In both acetylene cases, the concentration of Fe^{2+} doubles, ethylene increases by nearly 50%, while other samples follow less closely. Compared side by side would not be relevant in this situation.

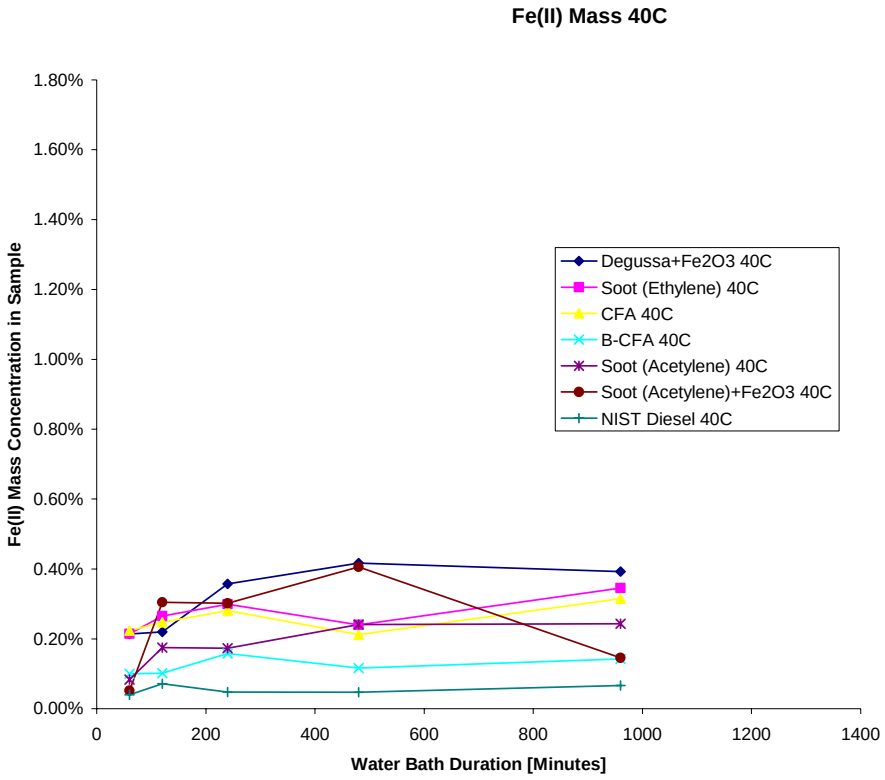

Figure 15. Fe^{2+} concentrations of different samples following acid extraction at 40 °C.

SUMMARY AND CONCLUSIONS

Elemental carbon reduces Fe^{3+} to Fe^{2+}. Seven different soot samples containing various amounts of Fe^{3+} were placed through an acid extraction process which verified this statement. More importantly, the time in which this happens was presented. At both temperatures this increase in Fe^{2+} happened very quickly. This indicates that Fe^{2+}, the same ionic state of iron that has been known to cause DNA destruction as well as additional health concerns, achieves its final concentration rapidly. In addition, the samples with the highest concentration of Fe^{2+} also had the largest total iron mass in its system. Meaning those samples with highest threat potential achieves this condition the fastest. These mass concentrations gradually increased or stayed constant over time and when plotted next to each other, this pattern attempts to show how these samples would act over a longer time duration at 40 °C.

In conclusion, further testing needs to be done to gain a complete understanding of this iron reduction process and hopefully finding the means to minimize its negative affects on humans with the help of this information.

RECOMMENDATIONS FOR FUTURE WORK

Additional testing at previous test conditions to validate current measurement, rectify any misconception of samples that were subjected to minimal testing, and to ultimately obtain an extensive library of test data.

Currently BET surface area analysis has been done on three of the samples that have been presented. It would be advantageous to test the remaining samples to provide a complete comparison.

Further instrumental analysis is also limitless. Since samples with larger hydrophilic group numbers which possessed higher surface area were capable of absorbing more Fe^{3+} (Uchida et al., 1961) functional group measurement might be the next important avenue to pursue. Transmission Electron Microscopy, TEM, and Scanning Electron Microscopy, SEM would determine the morphology of these particles. The distribution of the elements in the particles will be determined using Energy Dispersive X-ray Spectroscopy, EDS, mapping. Mössbauer should also be done on the remaining sample not already tested. Thermogravimetric Analysis, TGA, would be a simple test that would determine changes in weight in relation to change in temperature.

While there are an unlimited number of health studies that could be conducted, it would be best to start small such as continue cell culture studies could eventually lead to equivalent human specimens.

REFERENCES

Brewer, G. (2006). Iron and copper toxicity in diseases of aging, particularly atherosclerosis and Alzheimer's disease. *Experimental Biology and Medicine* 232:323-335.

Bruins, M., Kapil, S., and Oehme, F. (2000). Microbial resistance to metals in the environment. *Ecotoxicol Envrion. Safety* 45:198-207

Cass, G., Hughes, L., Bhave, P., Kleeman, M., Allen, J., and Salmon, L. (2000). The chemical composition of atmospheric ultrafine particles. *Philosophical Transactions of the Royal Society of London Series a-Mathematical Physical and Engineering Sciences* 358:2581-2592.

Cho, A., Sioutas, C., Miguel, A., Kumagai, Y. Schmitz, D., Singh, M., et al. (2005). Redox activity of airborne particulate matter at different sites in the Los Angeles basin. *Environmental Research* 99:40-47.

De Vizcaya-Ruiz, A., Gutierrez-Castillo, M., Uribe-Ramirez, M., Cebrian M., Mugica-Alvarez, V., Sepulveda, J., et al. (2006). Characterization and in vitro biological effects on concentrated particulate matter from Mexico City. *Atmospheric Environment* 40:S583-S592.

Dockery, D., Pope, C., Xu, X., Spengler, J., Ware, J., Fay, M., Ferris, B., and Speizer, F. (1993). An association between air-pollution and mortality in 6 United-States cities. *New England Journal of Medicine* 329:1753-1759.

Donaldson, K., Tran, L., and Jimenez, L. (2005). Combustion derived nanoparticles: a review of their toxicology following inhalation exposure 1. *Part Fibre Toxicol* 2:10.

Fenoglio, I., Prandi, L., Tomatis, M., and Fubini, B. (2001). Free radical generation in the toxicity of inhaled mineral particles: the role of iron speciation at the surface of asbestos and silica. *Redox Report* 6:235-241.

Fernandez, A., Wendt, J., Wolski, N., Hein, K., Wang, S., and Witten, M. (2003). Inhalation health effects of fine particles from the co-combustion of coal and refuse derived fuel. *Chemosphere* 51:1129-1137.

Filho, A., Hoffmann, M., and Meneghini, R. (1983). Cell killing and DNA damage by hydrogen peroxide are mediated by intracellular iron. *Biochem. J.* 218:273-275.

Fu, R., Zeng, H., and Lu, Y. (1993). Studies on the mechanism of the reaction of activated carbon fibers with oxidants. *Carbon* 32:593-598.

Geller, M., Ntziachristos, L., Mamakos, A., Samaras, Z., Schmitz, D., Froines, J., and Sioutas, C. (2006). Physicochemical and redox characteristics of particulate matter (PM) emitted from gasoline and diesel passenger cars. *Atmospheric Environment* 40:6988-7004.

Huggins, F., Huffman, G., and Robertson, J. (2000). Speciation of elements in NIST particulate matter SRMs 1648 and 1650. *Journal of Hazardous Material.* 74:1-23.

Iijima, S. (1991). Helical microtubes of graphitic carbon *Nature* 254:56.

Jayman, T., Sivasubramaniam, S., and Wijedasa, M. (1975). Elimination of interference from aluminum in the determination of total iron in soil and plant materials using 1,10-phenanthroline reagent. *Analys.* 100:716-720

Knaapen, A., Shi, T., Borm, P., and Schins, R. (2002). Soluble metals as well as the insoluble particle fraction are involved in cellular DNA damage induced by particulate matter. *Molecular and Cellular Biochemistry* 234:317-326.

Kunzli, N., Mudway, I., Gotschi, T., Shi, T., Kelly, F., Cook, S., et al. (2006). Comparison of oxidative properties, light absorbance, and total and elemental mass concentration of ambient PM 2.5 collected at 20 European sites. *Environmental Health Perspectives* 114:684-690.

Lam, C., James, J., McCluskey, R., Arepalli, S., and Hunter, R. (2006). A review of carbon nanotube toxicity and assessment of potential occupational and environmental health risks. *Critical Reviews in Toxicolog.* 36:189-217.

Limbach, L., Wick, P., Manser, P., Grass, R., Bruinink, A., and Stark, W. (2007). Exposure of engineered nanoparticles to human lung epithelial cells: Influence of chemical composition and catalytic activity on oxidative stress. *Environ. Sci. Technol*. 41:4158-4163.

Majestic, B., Schauer, J., Shafer, M., Turner, J., Fine, P., Singh, M., and Sioutas, C. (2006). Development of a wet-chemical method for the speciation of iron in atmospheric aerosols. *Environmental Science & Technolog.* 40:2346-2351.

Miglierini, M, and Petridis, D. *Mössbauer Spectroscopy in Materials Science*. Dordrecht: Kluwer, 1999.

Oberdorster, G., (2001). Pulmonary effects of inhaled ultrafine particles. *International Archives of Occupational and Environmental Health* 74:1-8.

Oberdorster, G., Gelein, R., Ferin, J., and Weiss, B. (1995). Association of particulate air-pollution and acute mortality-involvement of ultrafine particles. *Inhalation Toxicology* 7:111-124.

Oberdorster, G., Oberdorster, E., and Oberdorster, J. (2005). Nanotoxicology: an emerging discipline evolving from studies of ultrafine particles. *Environmental Health Perspectives* 113:823-839.

Prandi, L., Bodoardo, S., Penazzi, N., and Fubini, B. (2001). Redox state and mobility of iron at the asbestos surface: a voltammetric approach. *Journal of Materials Chemistry* 11:1495-1501.

Samet, J., Dominici, F., Curriero, F., Coursac, I., and Zeger, S. (2000). Fine particulate air pollution and mortality in 20 US cities, 1987-1994. *New England Journal of Medicine* 343:1742-1749.

Schwartz, J. and Neas, L. (2000). Fine particles are more strongly associated than coarse particles with acute respiratory health effects in schoolchildren. *Epidemiology* 11:6-10.

Smith, K., Veranth, J., Hu, A., Lighty, J., and Aust, A. (2000). Interleukin-8 levels in human lung epithelial cells are increased in response to coal fly ash and vary with the bioavailability of iron, as a function of particle size and source of coal. *Chemical Research in Toxicology* 13:118-125.

Tamura, H., Goto, K., Yotsuyanagi, T., and Nagayama, M. (1974). Spectrophotometric determination of Iron(II) with 1,10-phenanthroline in the presence of large amounts of Iron(III). *Talanta* 21:314-318.

Tuomainen, T., Loft, S., Nyyssonen, K., Punnonen, K., Salonen., J., and Poulsen, H. (2007). Body iron is a contributor to oxidative damage of DNA. *Free Radical Research* 41:324-328.

Uchida, M., Shinohara, O., Ito, S., Kawasaki, N., Nakamura, T., and Tanada, S. (1961). Reduction of Iron(III) ion by activated carbon fiber. *Journal of Colloid and Interface Science* 224:347-350

Van Maanen, J., Borm, P., Knaapen, A., Van Herwijnen, M., Schilderman, P., Smith, K., Aust, A., Tomatis, M., and Fubini, B. (1999). In vitro effects of coal fly ashes: hydroxyl radical generation, iron release, and DNA damage and toxicity in rat lung epithelial cells. *Inhalation Toxicolog.* 11:1123-1141.

Veranth, J., Smith, K., Aust, A., Dansie, S., Griffin, J., Hu, A. A., Huggins, M., and Lightly, J. (2000). Coal fly ash and mineral dust for toxicology and particle characterization studies: Equipment and methods for PM2.5-and PM1-enriched samples. *Aerosol Science and Technology* 32:127-141.

Veranth, J., Smith, K., Huggins, F., Hu, A., Lighty, J., and Aust, A. (2001). Mössbauer spectroscopy indicates that iron in an aluminosilicate glass phase is the source of the bioavailable iron from coal fly ash. *Chemical Research in Toxicology* 13:161-164.

Verbeek, F. (1961). Determination of traces of bismuth in copper by anodic stripping voltammetry. *Bull. Soc. Chim. Belg.* 70:423.

Weinberg, E. (2007). Iron loading in humans: A risk factor for enhanced morbidity and mortality. *Journal of Nutritional & Environmental Medicine* 16:43-51.

Zhou, Y., Zhong, C., Kennedy, I., Leppert, V., and Pinkerton, K. (2003). Oxidative stress and NF kappa B activation in the lungs of rats: a synergistic interaction between soot and iron particles. *Toxicology and Applied Pharmacology* 190:157-169.

Zhuang, G., Yi, Z., and Wallace, G. (1995). Iron(II) in rainwater, snow, and surface seawater from coastal environment. *Mar. Chem.* 50:41-50.

APPENDIX A

SAFE OPERATING PROCEDURES

The safe operating procedures include pre-experiment activities, the experimental, and the post test activities.

Pre-Experiment Activities

The following activities were carried out as pre-experiment activities.

Gas and Electrical Connections

- It was made sure that all the mass flow controllers, MFCs, are turned off, the gas cylinder main valves are shut off.
- The gas lines connections were checked to make sure they were attached to the correct cylinders.
- Connections were made between the desired MFCs and the gas lines from the MFCs to the burner. It was made sure that the gas type and maximum flow rate information in the mass flow control programmer/display (main control box) is correct for every MFC.
- It was verified that the gases are led to the correct inlets of the burner.

Burner Cleaning

- Any initial contamination from the burner was cleaned using brushing, washing and blowing etc. additional care was taken when disconnecting the burner to avoid damage.

Experiment Activities

The following activities are carried out with the start of the experiment.

- Start of synthesis
- It was made sure that a correct set point is set for fuel gas. The fuel gases supply was started and was allowed to run for 30 seconds.
- The front end of the 'synthesis chamber' was then closed with a plexi-glass cover, and the flame is started with a lighter.
- After noticing a steady flame formation the vacuum pump is also started to start the process of particle collection.

Sampling

- A filtration device was used to undertake the process of sampling. Care was taken in positioning the sapling tube so that no overheating occurs.

Shutdown

The following 'shutdown' procedure was followed**:**

- The vacuum pump is turned off first.
- Next turn off all gases by pressing "OFF" "ALL" on the mass flow controller. Then turn off the individual channels.
- Shut the main valve of each compressed gas cylinder.
- Disconnect the $FeCO_5$ and place it back in the storage closet.

Sample retrieval

- The filter holder was then removed by disconnecting the nozzle tube that is attached to the back of the filter holder from the vacuum line. Special care was taken while handling the filter holder because of the high temperature of the filter holder. The filter holder is cooled to a safe temperature before retrieving the filter.
- A Petri dish was made ready for storing the filter sample.
- The filter holder while maintaining its upright position (filter facing up) was removed. The filter is then exposed. A medical inhalation mask is worn and the filter was then picked up with a pair of sharp tweezers. Special care is taken to avoid breaking or cracking the filter. The filter sample is then transferred to wax paper were the sample is weighted and correctly labeled for future use.

Post Test Activities

- It was made sure that the gas cylinders are shut off.
- It was made sure that all used glassware was properly cleaned and placed on the drying rack available for the next user.
- It was made sure that all spills and debris has been cleaned.

APPENDIX B

METHODOLOGY

All the analysis preformed on the samples were subjected to many different chemical combinations and concentrations. Research and careful thought was placed into all of these decisions. The following are justifications to the final quantities used.

Phenanthroline

Once experiments commenced, errors surfaced immediately. It was determined that the initial procedure to create the phenanthroline was flawed. The 10% isopropyl alcohol in the 1,10-phenanthroline DI water solution was not pungent enough to completely dissolve the 1,10-phenanthroline in the allotted time. The end effect was accentually no phenanthroline being introduced to the system, causing no color development as show below in Figure 16.

Figure 16. Initial phenanthroline mixing errors led to no color development within solutions.

To resolve this situation, acetone replaced the isopropyl; the solution was allowed to completely dissolve upon observation instead of following the recommended time, as well as a slight alteration in the. Lastly, 1,10-phenanthroline and hydroquinone standard solutions will be made and wrapped in aluminum foil; however this too would be changed later. The end effect can be seen in Figure 17, where color is fully developed and proper data recovery can begin.

Figure 17. Proper color development following corrections to initial phenanthroline procedure.

The order which phenanthroline is introduced is also critical; Tamura *et al. 1974* reported that Verbeek's (1961) decision to add the phenanthroline prior to other chemicals was incorrect. In the presents of sunlight, the Fe^{3+}-phenanthroline combination undergoes a photoreductions. By adding the phenanthroline first, any expose to sunlight during the addition of reagents will not affect the determination. The hydroquinone and phenanthroline solutions were previously made and were kept in the chemical storage cabinet in dark amber bottles to minimize chemical color development from this expose to sunlight. While nature of a phenanthroline solution is relatively stable. Additionally, the color intensity increases with time, so as suggested that the solution was renewed every 4 weeks (Tamura et al., 1974).

Not only is the color is time important to the phenanthroline solution the minimum concentration must also be above a specific level. This adapted Figure 18 determines that the minimum required amount for proper color development of 1,10-Phenanthroline is 1 mL for every 25 mg of Iron.

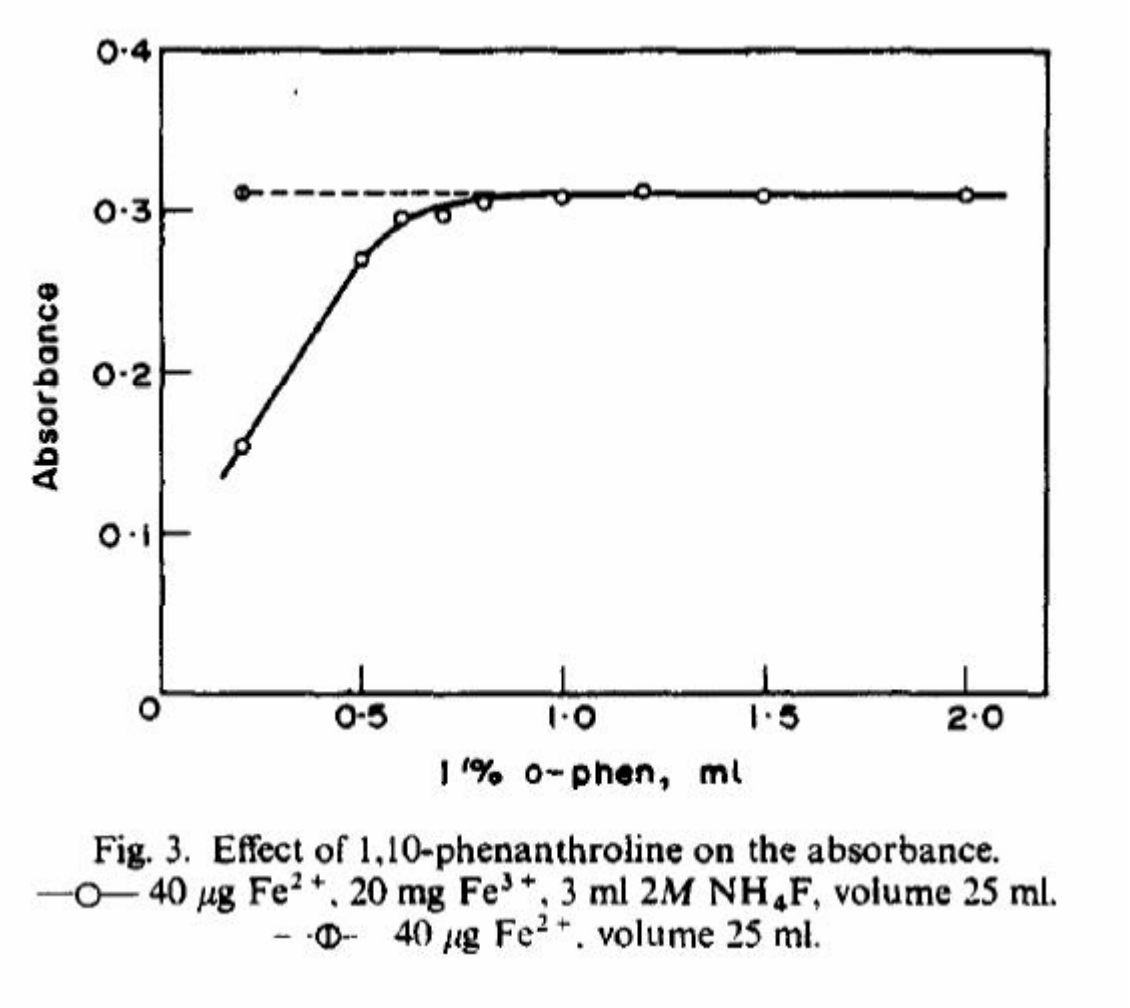

Fig. 3. Effect of 1,10-phenanthroline on the absorbance.
—○— 40 μg Fe^{2+}, 20 mg Fe^{3+}, 3 ml 2*M* NH_4F, volume 25 ml.
– ·Φ– 40 μg Fe^{2+}, volume 25 ml.

Figure 18. Effect of 1,10-phenanthroline on absorbance.

Several months into the experimental process, it was decided to change to cover of the acid digestion solution from aluminum foil to a plastic wrap. Jayman (1975) describes how the introduction of aluminum in a solution with phenanthroline caused the absorbance reading to increase and offer a false measurement. While aluminum was not intentionally introduced to our solutions, this precaution was taken to eliminate unforeseen error. Later measurements were then compared to

initial values and were found to be the same, gathering that aluminum cover never combined with our acid extraction solution.

Acids

In an attempt to mimic the human body, different types of acids were used to digest the samples. Acetic acid was no longer used as a viable candidate for this study after a long streak of not producing readings. After that point sulfuric acid became the sole acid used. Several concentrations of sulfuric acid were tested and 20% in DI water became the staple concentration. This adapted Figure 19**,** shows that color intensity is stable as long as the 1 mL of acid is for every 25 mL solution of 40 μg of Iron. Given that Tamura's study was used to determine the relationship between sulfuric acid and ammonium fluoride concentrations, the same lessons were applied to our spectrophotometric method. Further indication that our model is relevant is the similarity in location of the pH values. Where the absorbance becomes linear, the declare value is between 3 and 2, as was in ours.

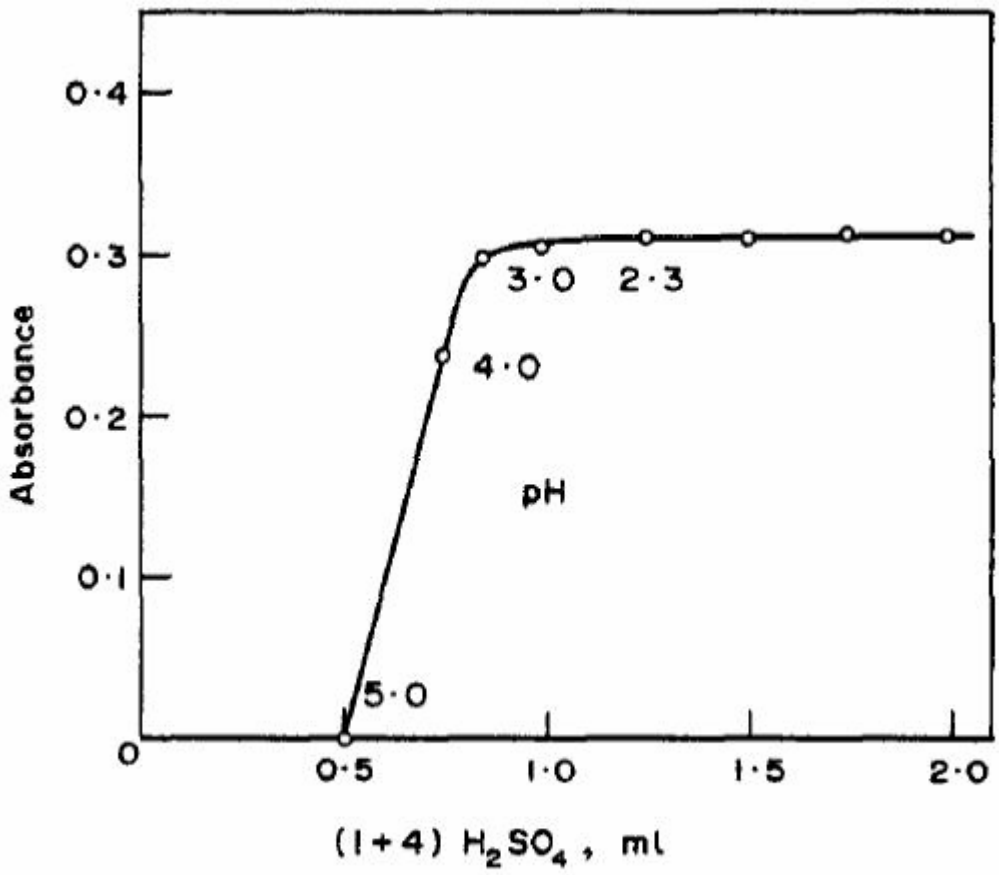

Fig. 1. Effect of sulphuric acid on the absorbance.
Volume 25 ml. 40 μg Fe^{2+}

Figure 19. Effect of sulphuric acid on absorbance.

APPENDIX C

REMAINING LABORATORY EQUIPMENT

Figure 20. Scientech digital scale.

Figure 21. Revolutionary Sciences water bath.

Figure 22. Barnstead Thermolyne tube furnace.

APPENDIX D

BET ANALYSIS FIGURES

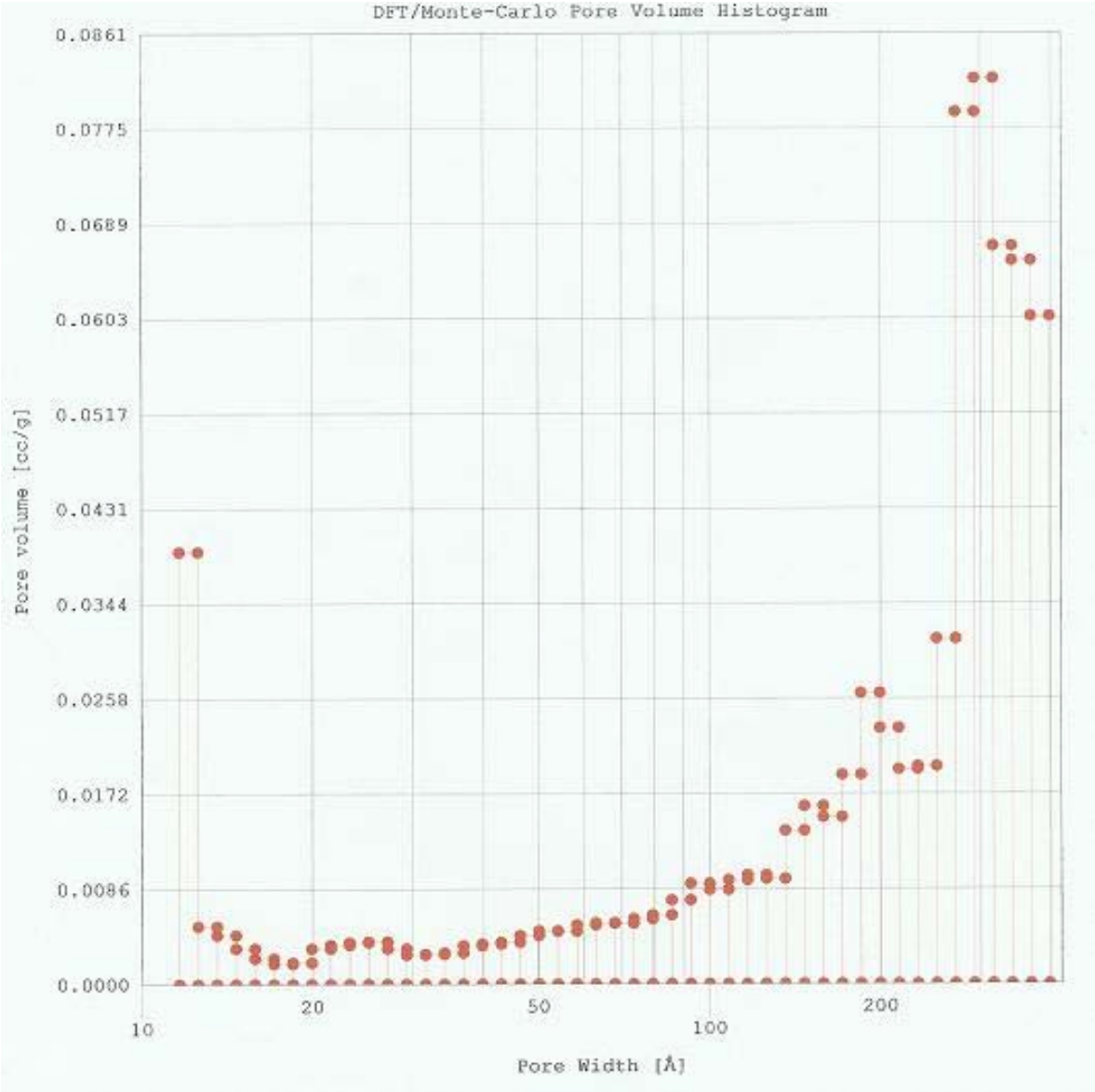

Figure 23. Degussa pore volume histogram.

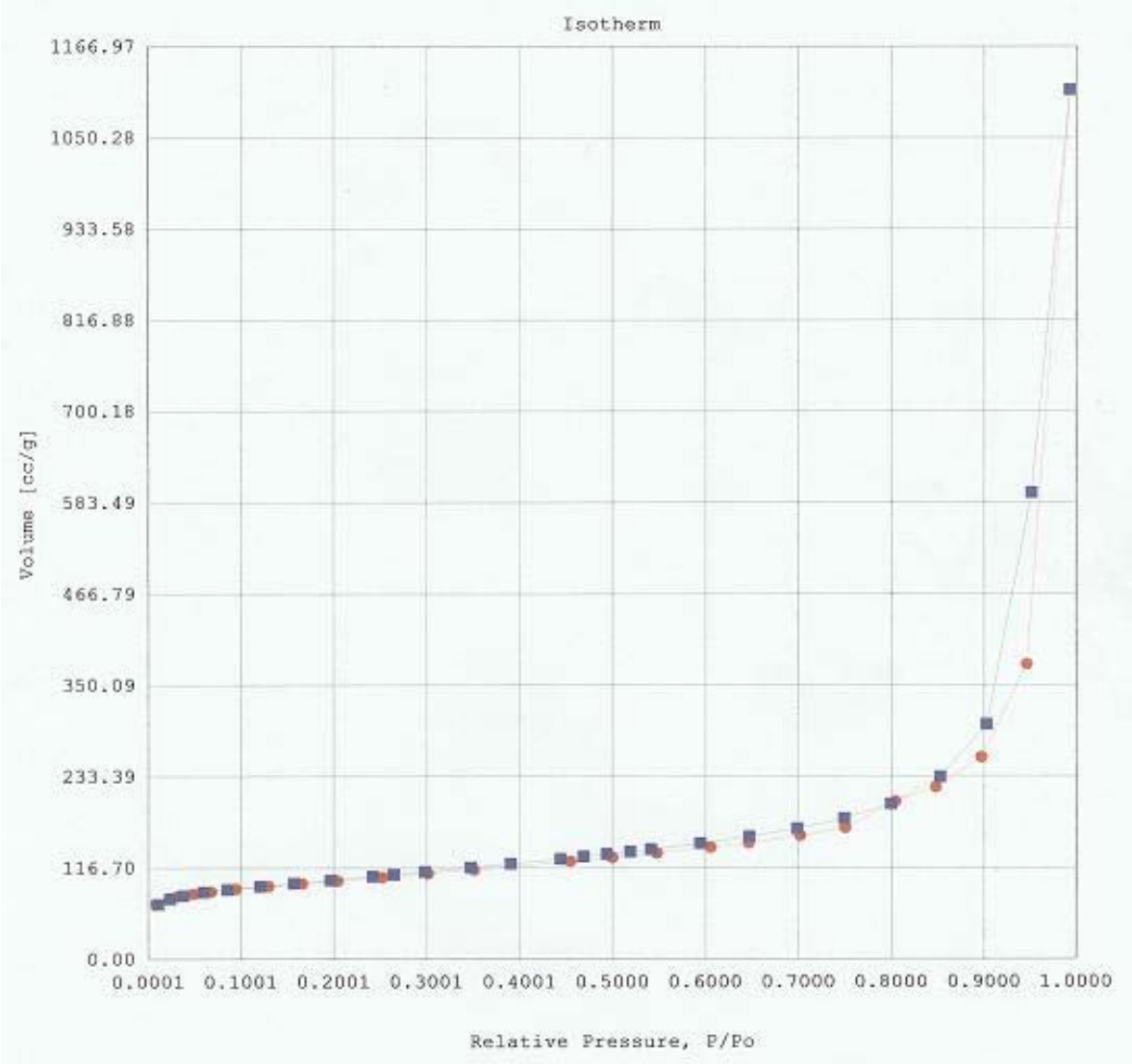

Figure 24. Degussa isotherm graph.

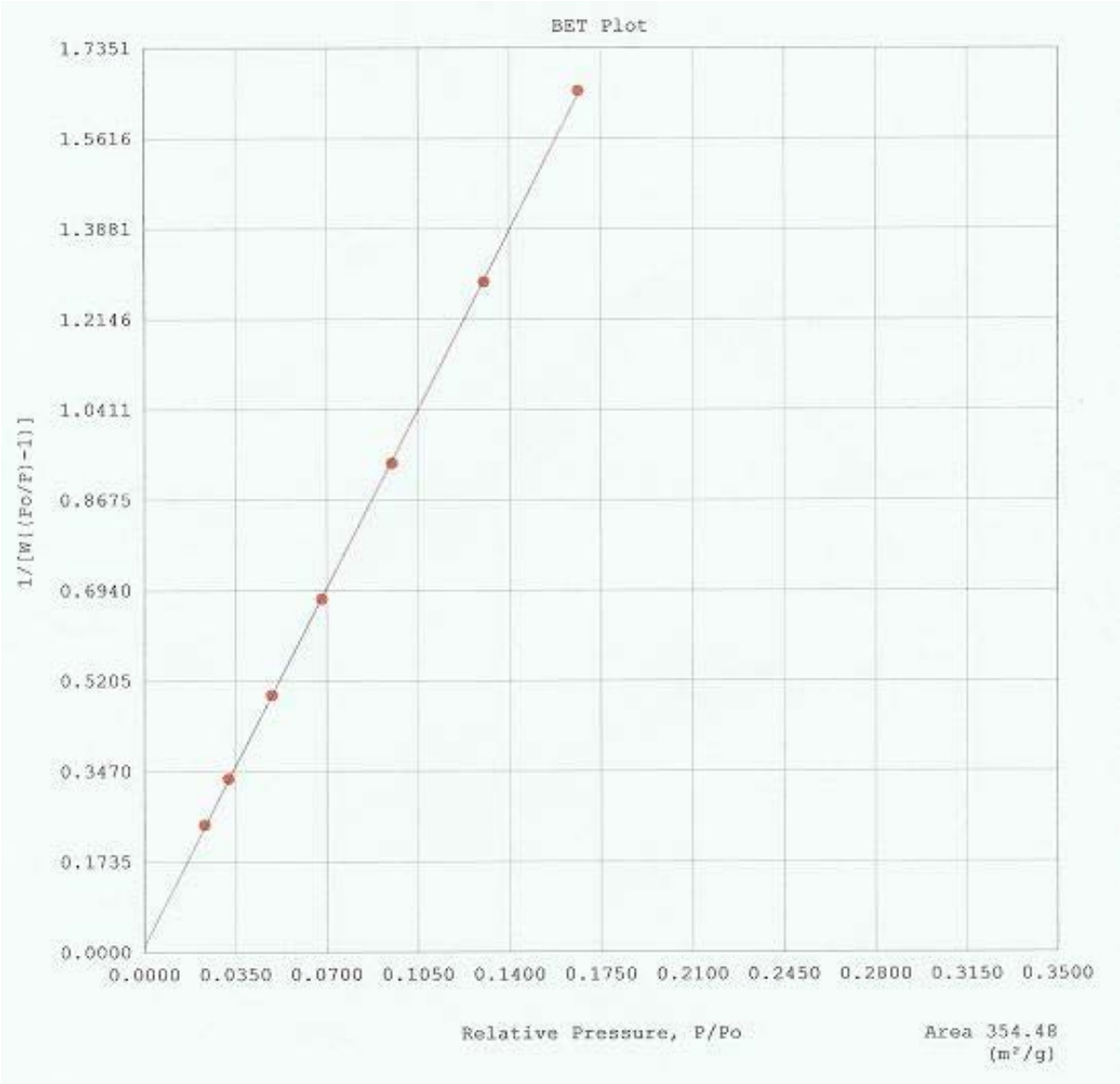

Figure 25. Degussa BET plot.

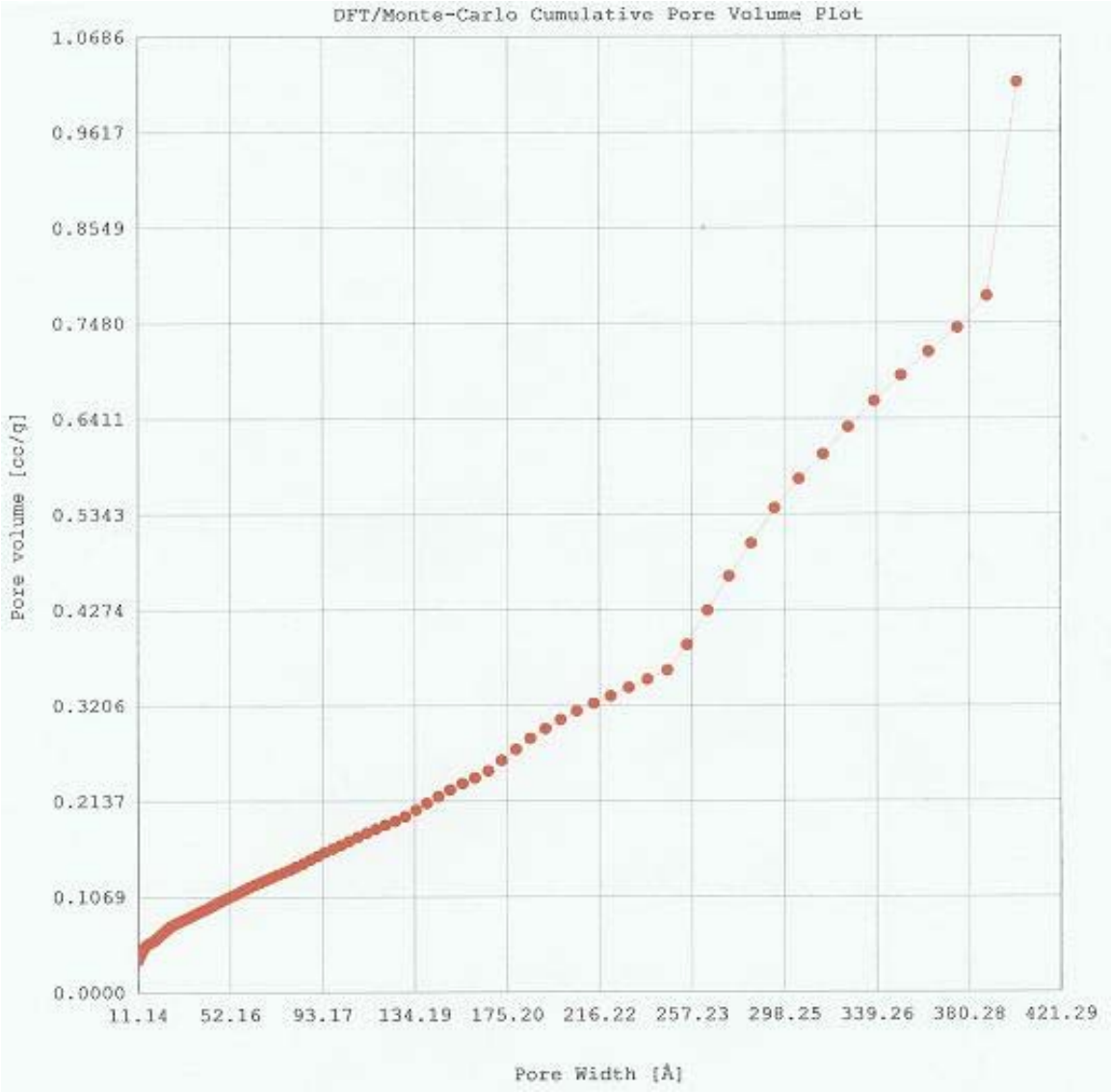

Figure 26. Degussa pore volume plot.

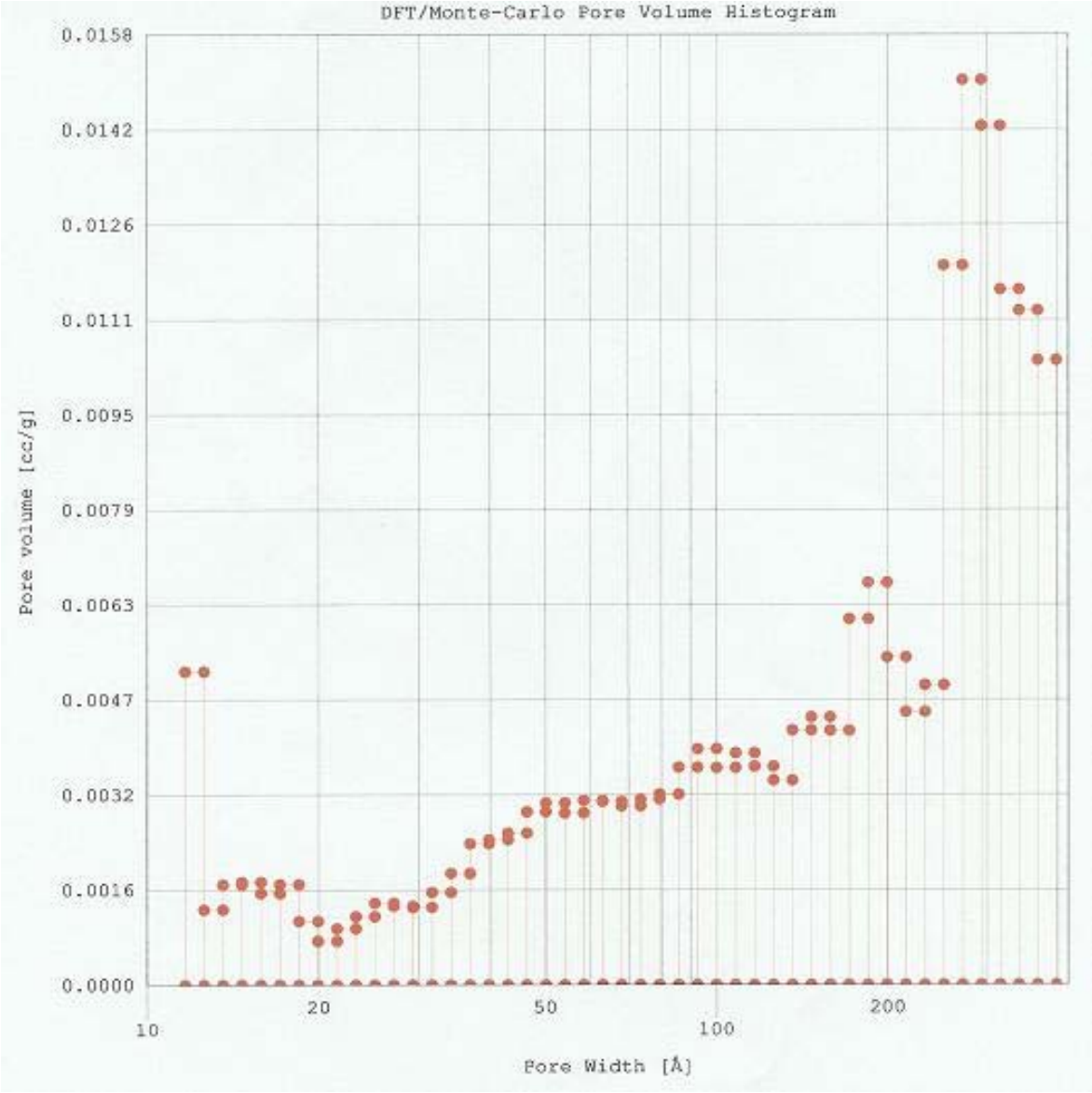

Figure 27. Diesel pore volume histogram.

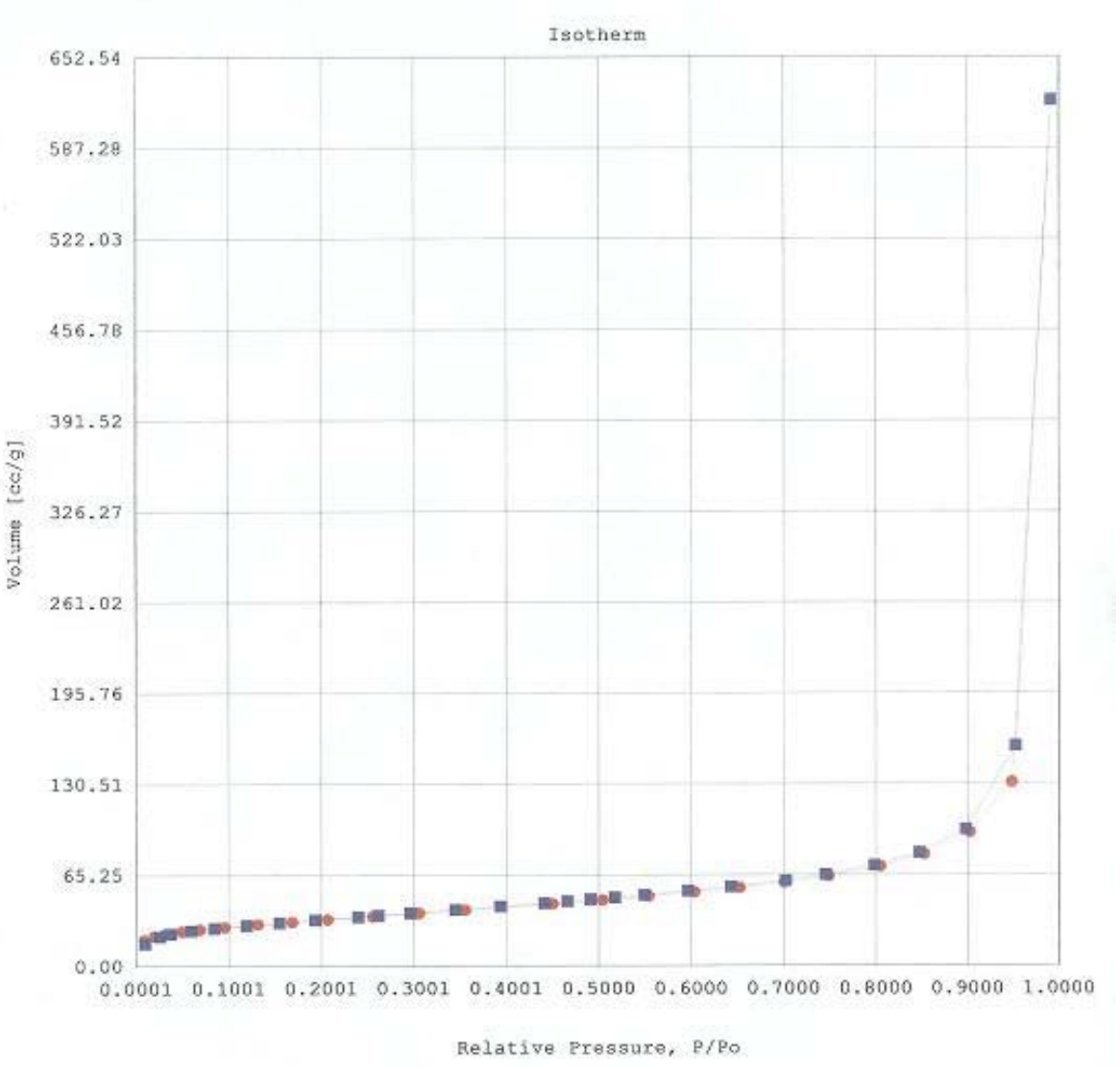

Figure 28. Diesel isotherm graph.

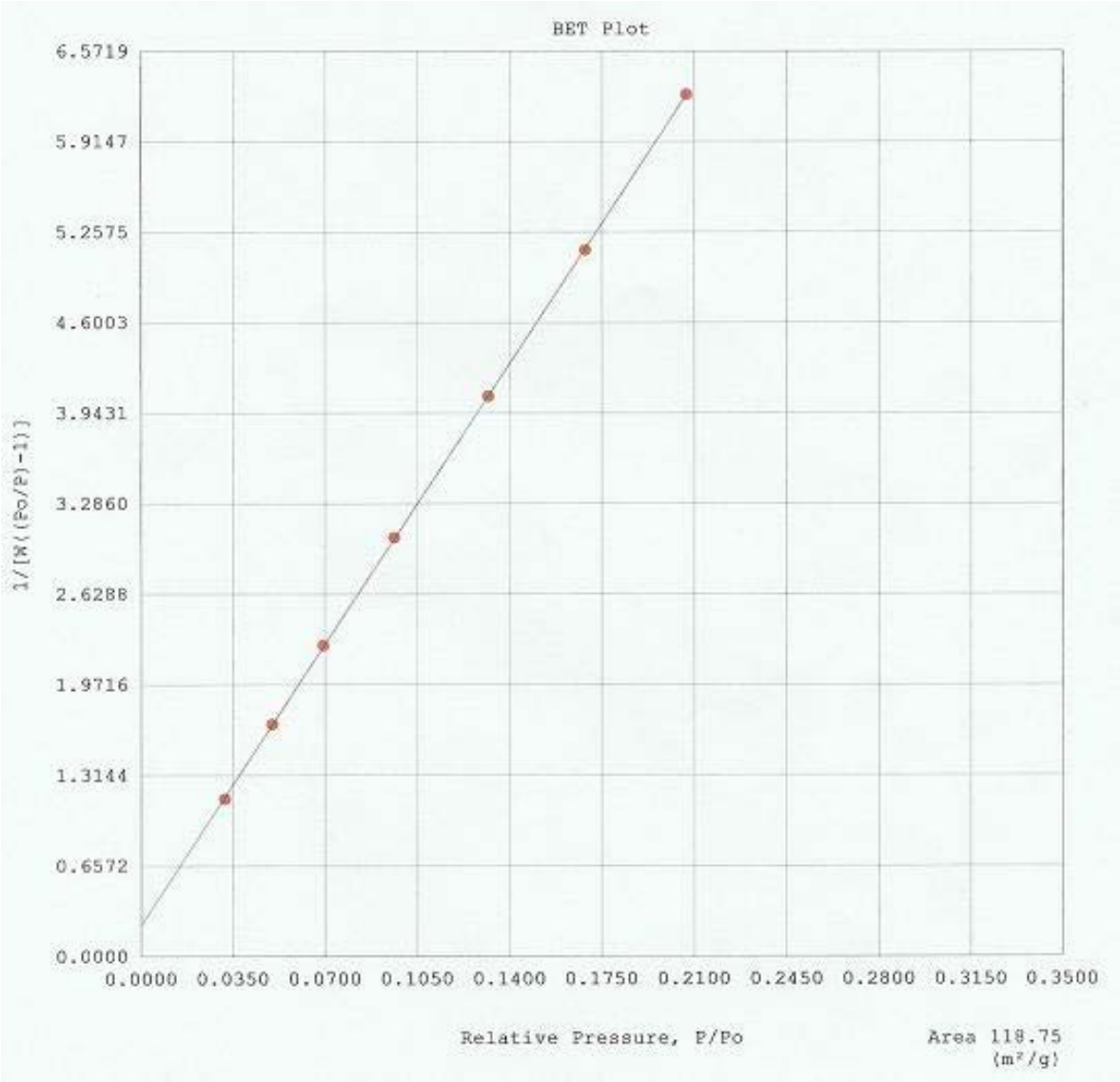

Figure 29. Diesel BET plot.

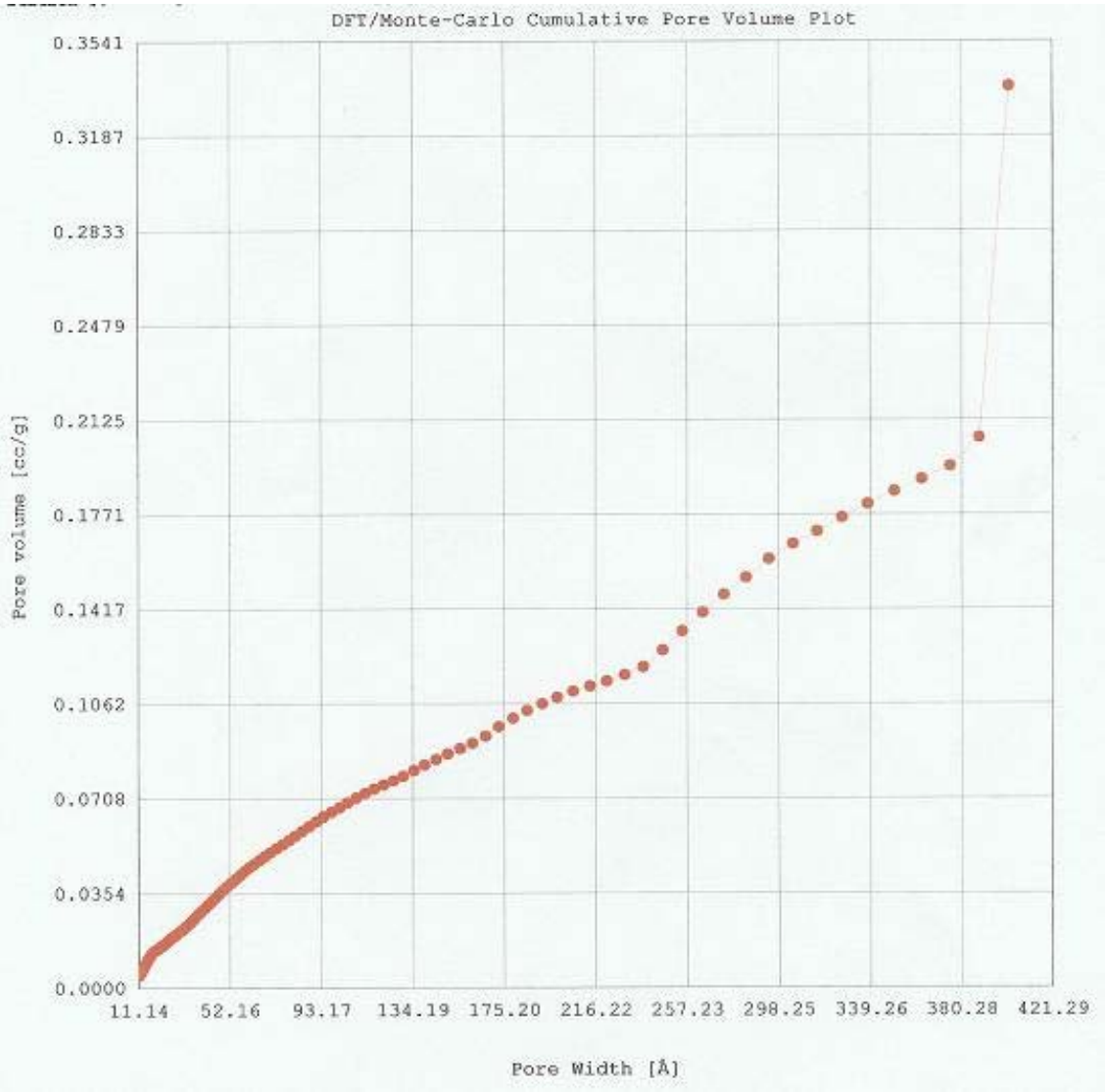

Figure 30. Diesel pore volume plot.

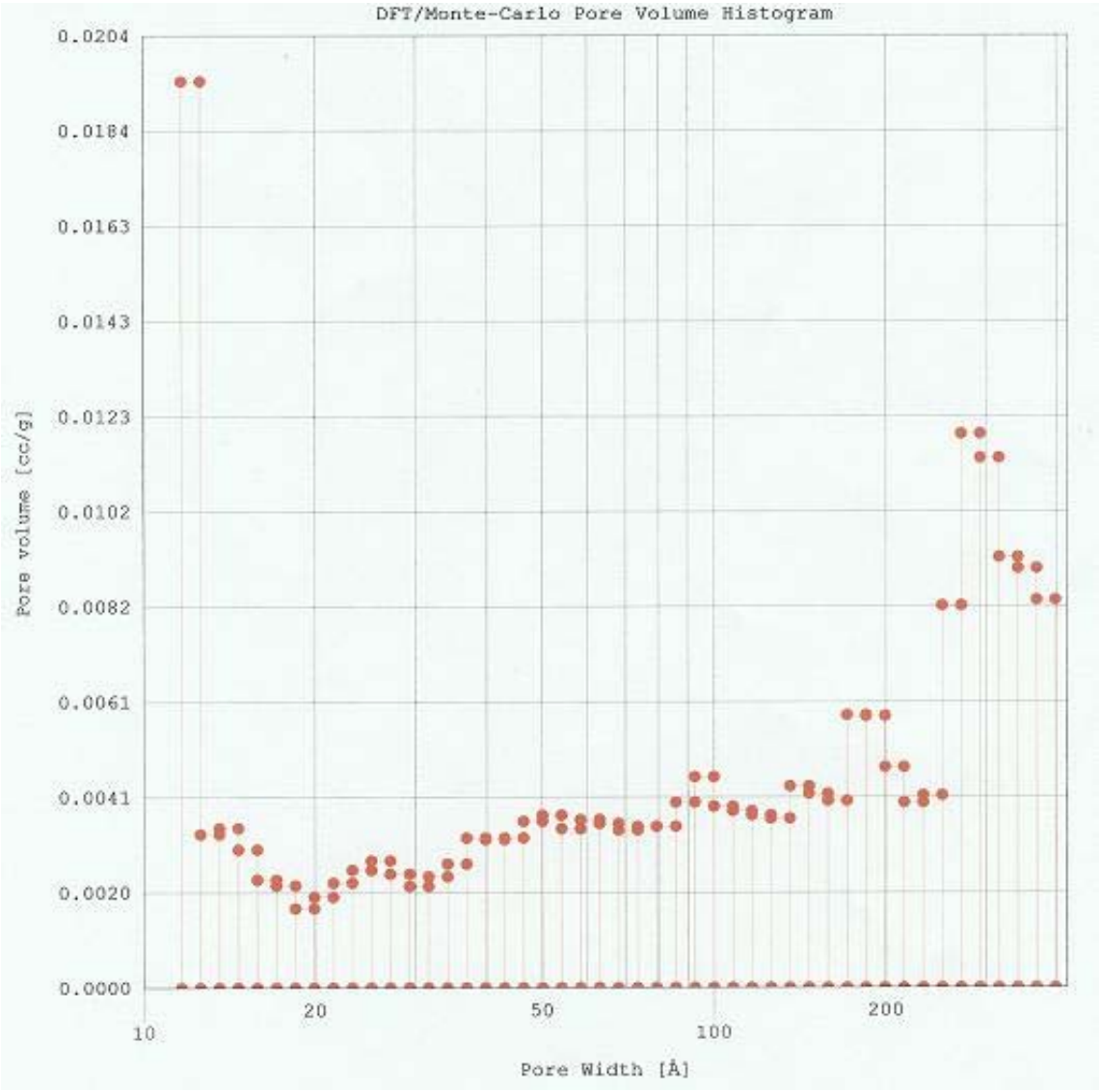

Figure 31. Soot-E pore volume histogram.

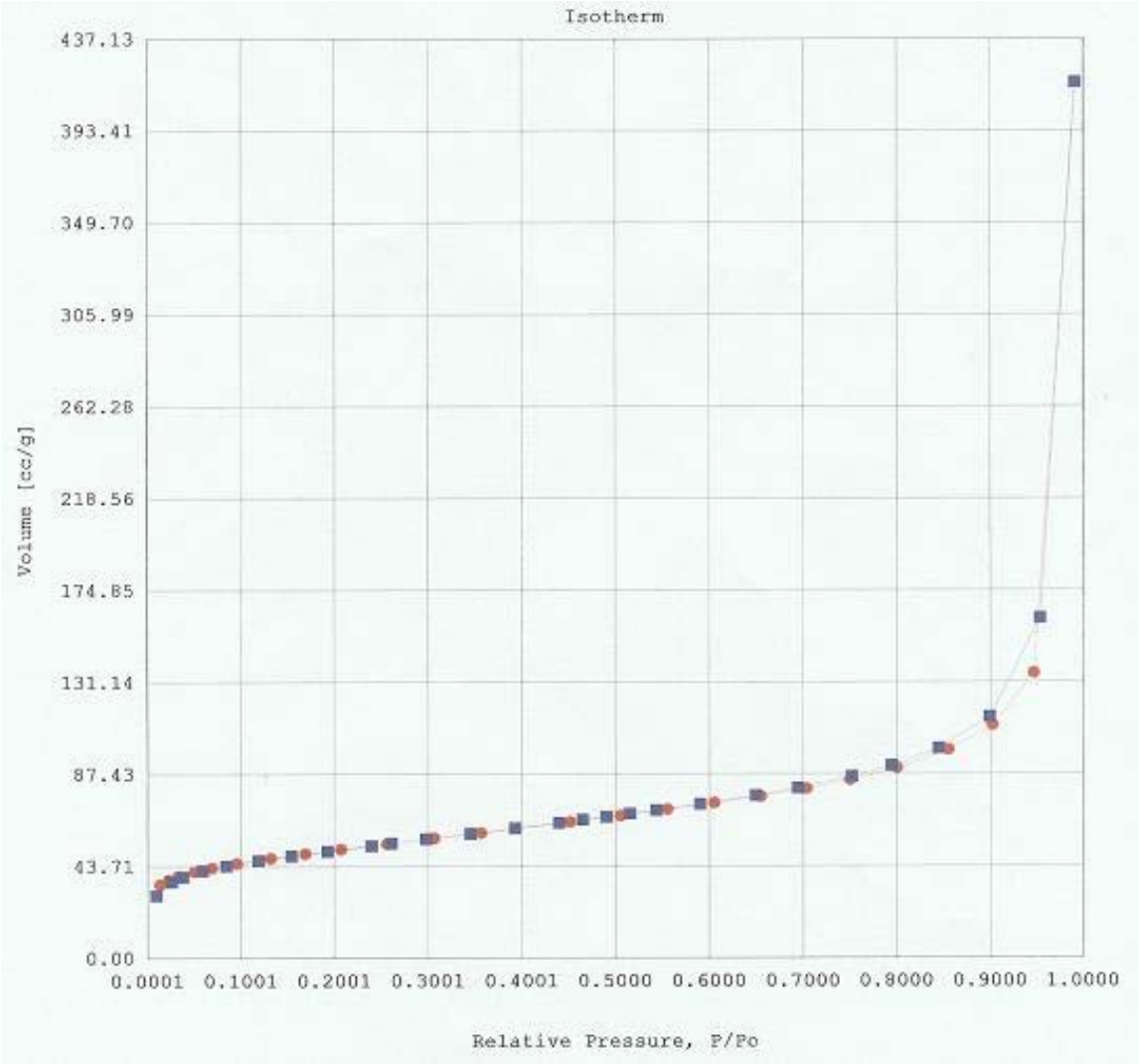

Figure 32. Soot-E isotherm graph.

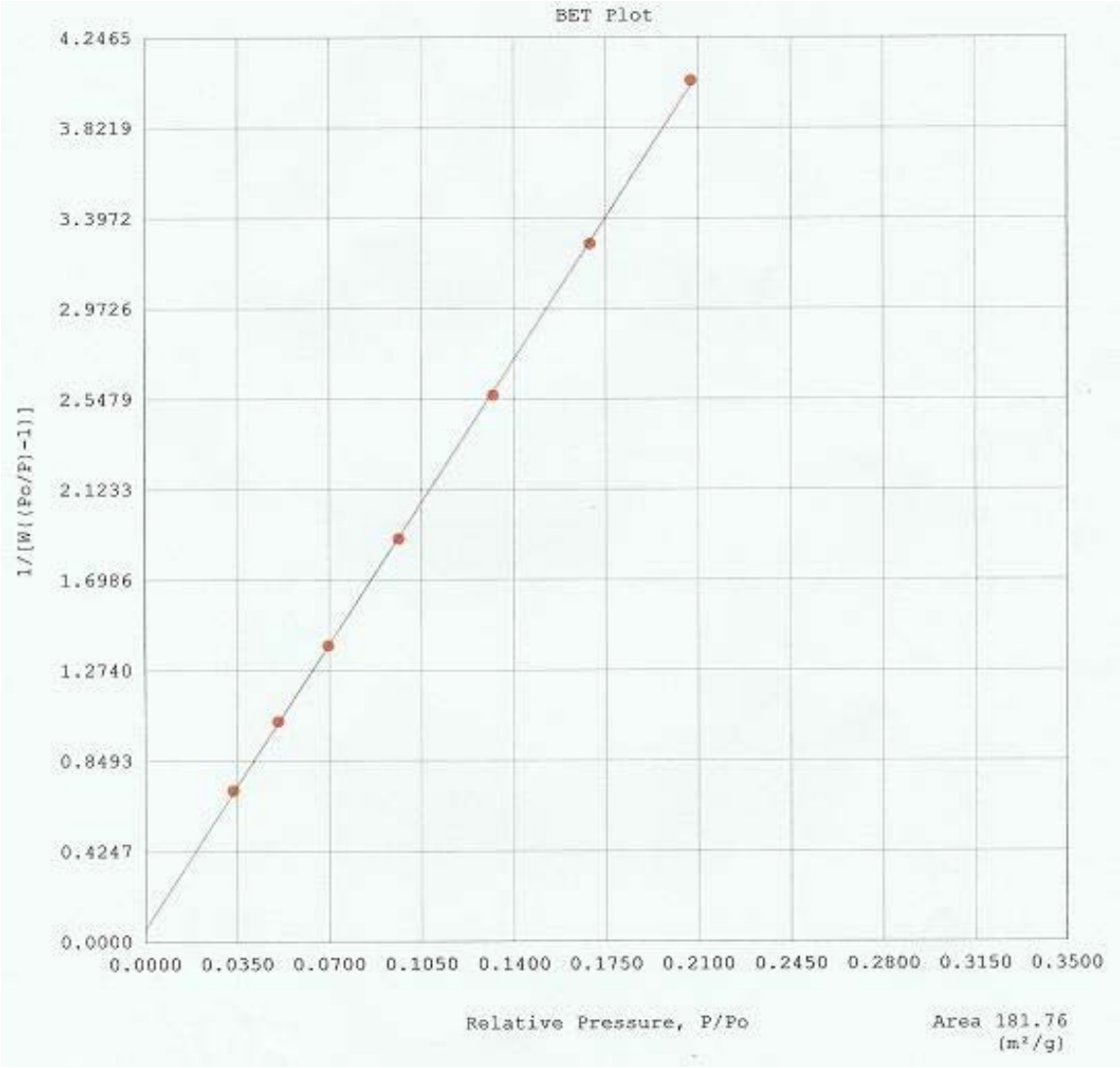

Figure 33. Soot-E BET plot.

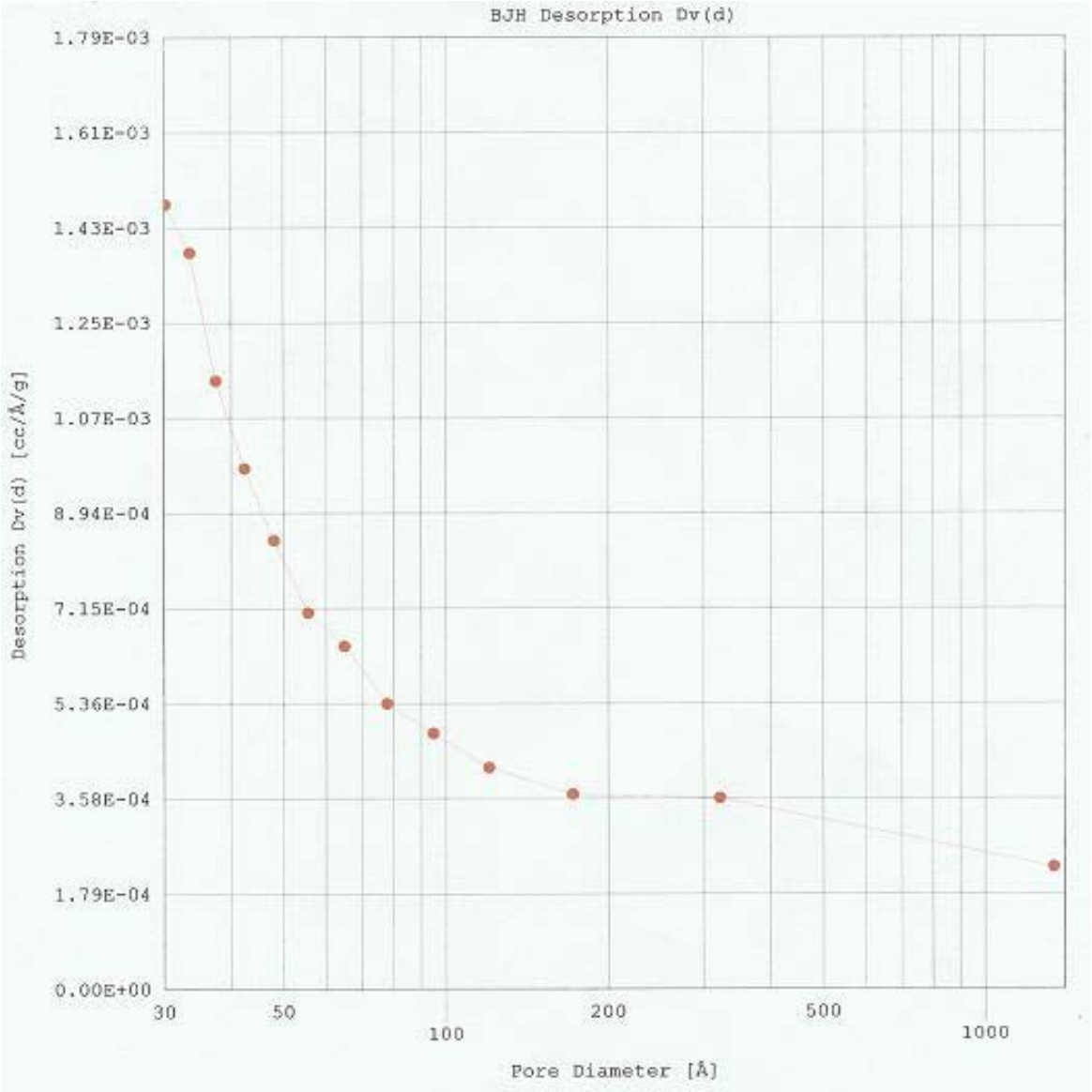

Figure 34. Soot-E desorption graph.

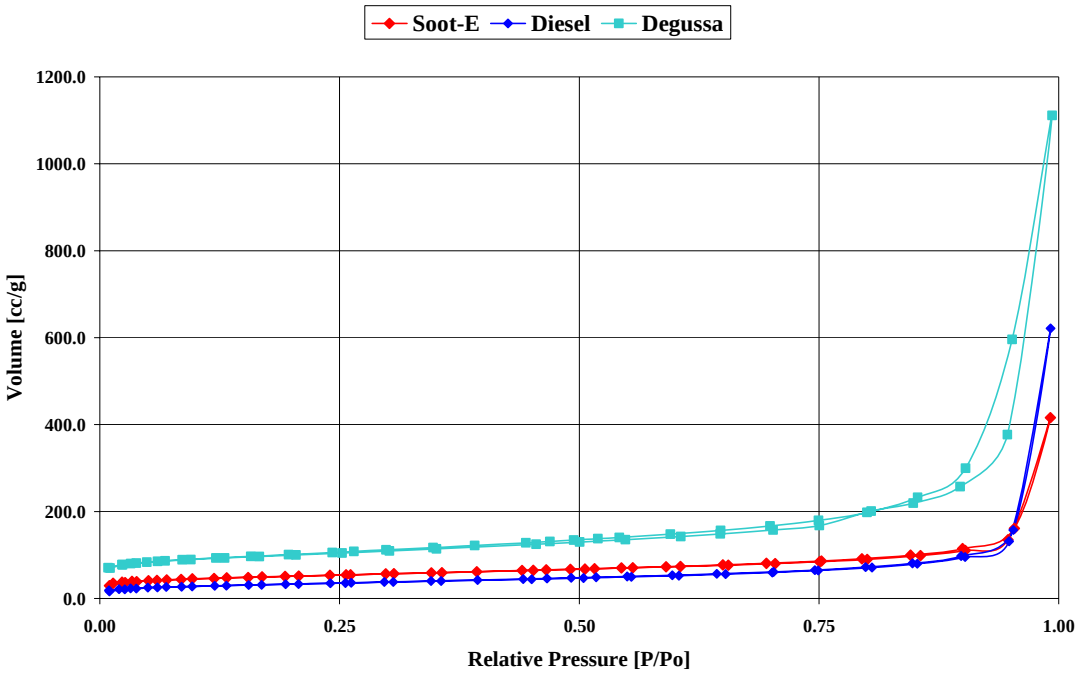

Figure 35. All isotherm graphs overlayed.

VITA

Name:	Stephen James Drake
Place of Birth:	Hutchinson, Kansas
Permanent Address:	Texas A&M University Department of Mechanical Engineering 3123 TAMU College Station, TX 77843-3123
Education:	M.S. Mechanical Engineering (May 2008) Texas A&M University College Station, Texas 77843 B.S. Mechanical Engineering (Spring 2005) Texas Christian University Fort Worth, Texas 76129
Work Experience:	8/06-5/08 Graduate Research Assistant Mechanical Engineering Department Texas A&M University College Station, Texas 77843 5/05-8/07 (Summers) Test Engineer Homeland Safety International 215 N. O'Connor Blvd. Ste. 200 Irving, Texas 75039 9/03-5/05 Student Internship KWS Manufacturing 3041 Conveyor Drive Burleson, Texas 76028